TECHNISCHE UNIVERSITÄT WIEN

AUTOMATION & CONTROL INSTITUTE
INSTITUT FÜR AUTOMATISIERUNGS- & REGELUNGSTECHNIK

Force Sensitive Teach-In for Industrial Robots

DIPLOMA THESIS

Conducted in partial fulfillment of the requirements for the degree of a

Diplom-Ingenieur (Dipl.-Ing.)

supervised by

Univ.-Prof. Dr. techn. A. Kugi
Dipl.-Ing. M. Schwegel

submitted at the

TU Wien
Faculty of Electrical Engineering and Information Technology
Automation and Control Institute

by
Hanspeter Augschöll
Matriculation number 01614826

Vienna, February 2020

Complex Dynamical Systems Group
A-1040 Wien, Gußhausstr. 27–29, Internet: https://www.acin.tuwien.ac.at

Die approbierte gedruckte Originalversion dieser Diplomarbeit ist an der TU Wien Bibliothek verfügbar.
The approved original version of this thesis is available in print at TU Wien Bibliothek.
TU Bibliothek Your knowledge hub WIEN

Preamble

I would like to express my deep gratitude to my supervisor Dipl.-Ing. Michael Schwegel for his support with words and deeds along my work on this project. I especially want to thank Univ.-Prof. Dr. techn. Andreas Kugi for the opportunity to work on this interesting topic. A special thank goes to Dipl.-Ing. Christian Hartl-Nesic who never hesitated to help me with my questions and share his immense knowledge on industrial robots. I also would like to thank the members of the institute who created such a pleasant work environment and my colleagues for their assistance and companionship.

Last but certainly not least I want to thank my family for their support throughout these years and most notably my partner Julia for her endless encouragement and motivation.

Vienna, February 2020

Die approbierte gedruckte Originalversion dieser Diplomarbeit ist an der TU Wien Bibliothek verfügbar.
The approved original version of this thesis is available in print at TU Wien Bibliothek.

Abstract

This thesis presents a new approach for the teach-in of a rope-winding task for a robot which includes position, orientation and force information. A manual teach-in tool was designed to facilitate the demonstration process.

Using the designed tool, the winding of a rope around arbitrarily placed rods can be demonstrated by an operator. A spool and a motor on the end-effector of the robot are used to exert the desired tension on the rope. Based on a path following control strategy with transverse feedback linearization the spool is guided along the path.

The control objectives for the spool position are formulated relative to the path using the parallel transport frame. The spool orientation is controlled using two degrees of freedom while the remaining degree of freedom is transferred to the null space of the primary task. This enables the definition of a subtask which controls the robot to take more beneficial configurations while traversing the path and facilitates the teach-in process.

The proposed strategy was validated on an experimental setup. It is shown that the teach-in tool provides an intuitive and robust means to demonstrate a task for being executable by the robot. The path following controller with the additional subtask is able to imitate the task with good accuracy.

Die approbierte gedruckte Originalversion dieser Diplomarbeit ist an der TU Wien Bibliothek verfügbar.
The approved original version of this thesis is available in print at TU Wien Bibliothek.
TU Bibliothek Your knowledge hub WIEN

Kurzzusammenfassung

Die vorliegende Arbeit präsentiert eine neue Teach-In-Methode, die neben Positions- und Orientierungsinformation auch Kraftinformation berücksichtigt. Im konkreten Fall wird das Teach-In einer Seilwickel-Aufgabe behandelt, welche anschließend von einem Roboter wiederholt wird. Dazu wurde ein Teach-In Werkzeug gebaut, welches diesen Demonstrationsprozess erleichtert.

Mit dem entworfenen Werkzeug wird das Wickeln eines Seils um beliebig angeordnete Stangen demonstriert. Eine am Flansch des Roboters montierte Seilspule an einem Motor wird dazu verwendet die während der Wiedergabe vorgegebene Seilspannung zu regeln. Mithilfe eines Pfadfolgereglers und einer exakten Linearisierung wird die Spule entlang des Pfades geführt.

Durch den Einsatz des Paralleltransport-Rahmens werden die Sollgrößen hinsichtlich der Spulenposition relativ zum Pfad formuliert. Zur Orientierungsregelung des Endeffektors werden lediglich zwei Freiheitsgrade verwendet, während ein Freiheitsgrad in den Nullraum projiziert wird. Dies ermöglicht es, eine untergeordnete Regelaufgabe zu formulieren, die den Roboter dazu bringt günstigere Konfigurationen einzunehmen, was den Demonstrationsprozess zusätzlich erleichtert.

Die vorgestellte Methode wurde anhand eines Aufbaus experimentell validiert. Es wird gezeigt, dass sich der Demonstrationsprozess mithilfe des Teach-In Werkzeugs intuitiv gestaltet und robust genug ist, um die eingelernte Aufgabe am Roboter wiederzugeben. Der Pfadfolgeregler mit der untergeordneten Regelaufgabe ist in der Lage, die definierten Regelziele mit guter Genauigkeit einzuhalten.

Die approbierte gedruckte Originalversion dieser Diplomarbeit ist an der TU Wien Bibliothek verfügbar.
The approved original version of this thesis is available in print at TU Wien Bibliothek.
TU Bibliothek Your knowledge hub WIEN

Contents

Die approbierte gedruckte Originalversion dieser Diplomarbeit ist an der TU Wien Bibliothek verfügbar.
The approved original version of this thesis is available in print at TU Wien Bibliothek.
TU Bibliothek Your knowledge hub WIEN

List of Figures

Die approbierte gedruckte Originalversion dieser Diplomarbeit ist an der TU Wien Bibliothek verfügbar.
The approved original version of this thesis is available in print at TU Wien Bibliothek.
TU Bibliothek Your knowledge hub WIEN

Acronyms

CAD Computer Aided Design.

CPU Central Processing Unit.

CS Coordinate System.

DH Denavit-Hartenberg.

DOF Degrees of Freedom.

FPS Frames per Second.

NIC Network Interface Card.

PbD Programming by Demonstration.

PFC Path Following Control.

PT Parallel Transport.

TCP Tool Center Point.

Die approbierte gedruckte Originalversion dieser Diplomarbeit ist an der TU Wien Bibliothek verfügbar.
The approved original version of this thesis is available in print at TU Wien Bibliothek.

1 Introduction

In recent years, a large number of robotic systems were introduced. This ranges from heavy-duty work for industrial robots in separate work cells to tasks where robots collaborate with an operator. To program a robot, different methods are used, from offline programming using *Computer Aided Design* (CAD) data to online programming by directly interacting with the robot. *Programming by Demonstration* (PbD) falls into the latter category in which teach-in describes the manual demonstration of a human operator, see [1]. Such methods are increasingly popular due to their simplicity for defining a sequence of movements. While teach-in can be done by guiding the robot to the desired positions other strategies involve the use of tools to ease the teach-in process. Apart from a path that defines different end-effector poses additional goals are desired, e. g., the application of a certain force along that path, in order to interact with the environment. Examples for such scenarios are packaging, assembly or drilling applications.

The goal of this thesis is the development of an approach for robot programming without the need of a highly trained operator to define a complex task. The present work considers a rope-winding task where a rope is wound around obstacles while exerting a desired tension. This is achieved by combining path and force information during teach-in for the task definition. Therefore, a manual tool is introduced that enables the concurrent recording of path and force information for the winding of a rope. The use of such a tool simplifies the programming process considerably. By manually guiding the tool and controlling the rope tension, the operator receives tactile feedback which enables an intuitive definition of the task. While the presented approach considers rope handling, the underlying ideas are transferable to other force-sensitive applications, e. g. assembly or machining tasks.

To verify the approach a KUKA LBR iiwa 14 R820 robot is used. The robot is equipped with a spool on a motor, mounted on the flange of the robot, which allows to wind a rope around rods while controlling the tension. To enable more beneficial robot configurations for different positions and orientations of the rods, the motor and the spool on the flange are tilted. In addition, a control strategy with a reduced task space is used. This enables the definition of a subtask in the null space of the primary task, whose goal it is to bring the joints of the robot near their neutral position, i. e. the zero position of each joint.

Die approbierte gedruckte Originalversion dieser Diplomarbeit ist an der TU Wien Bibliothek verfügbar.
The approved original version of this thesis is available in print at TU Wien Bibliothek.
TU Bibliothek Your knowledge hub WIEN

1.1 Literature Review

Since conventional methods for robot programming are quite time consuming and require highly trained operators, the simplification of the teach-in process of a robot has received considerable attention in recent years.

In [2], programming by demonstration is used to define a welding task. For this, a measuring probe, used to manually demonstrate the welding path, is tracked by an optical system. The resulting data is smoothed and a spline curve is generated for later reproduction by a robotic arm.

In [3, 4] kinesthetic programming (programming by guiding the robot's arm) is used for a combined recording of path and force information. A force/torque sensor, mounted between the robot flange and a tool, is used to measure the forces acting on the used tool. In addition, the utilized KUKA LWR4+ robot enables the measurement of the torque in each joint. This information is used during reenactment to apply the previously demonstrated contact forces while following the desired path. While in [4] the tool is a pencil to demonstrate writing, the work of [3] uses a manual plane to demonstrate wood planing.

A combination of programming methods (interaction and demonstration) using a manual tool is presented in [5]. The tool is captured by an optical system which tracks the movement. Additionally, the applied force during an assembly task (screwing bolts) is measured. The information is gathered and assembled into a knowledge graph. This establishes a relation between performed tasks and processed objects, hence obtaining a basic understanding of the consequences of the task in an assembly environment. This abstraction of acquired knowledge enables the transfer of knowledge for the handling of different objects. The approach is demonstrated by teaching the screwing of bolts in an assembly task to a robot.

To control the motion of a robot *path following control* (PFC) can be utilized. In combination with transverse feedback linearization PFC enables the separate control of the tangential and transversal motion relative to a path and hence can be applied to a variety of problems. In [6] necessary and sufficient conditions for feedback linearization to exponentially stabilize a periodic orbit are introduced. Further application of this methodology is covered in [7] and [8]. In [7], transverse feedback linearization is used in a magnetically levitated system. The systems output is driven to a desired path with a transversal controller while the speed on the path is controlled via a tangential controller. In [8], the same strategy is applied to a five-bar robotic manipulator to bring the end-effector to a desired curve and stabilize the movement along the path.

A further extension of this method is introduced in [9] where framed parametrized curves are used to define a path. The Frenet-Serret frame is utilized to construct a base in every point of a given curve. By applying a coordinate transformation the system output is mapped to the newly generated set of coordinates and thereby splits the dynamics into a transversal and tangential motion relative to a given path. With this approach also intersecting curves are possible. A drawback of this approach is that the Frenet-Serret frame is undefined when the curvature of the path is zero. This problem is solved in [10] using the *parallel transport* (PT) frame for the construction of an orthonormal base. The approach is combined with compliance control and validated on a DELTA robot.

Die approbierte gedruckte Originalversion dieser Diplomarbeit ist an der TU Wien Bibliothek verfügbar.
The approved original version of this thesis is available in print at TU Wien Bibliothek.
TU Bibliothek Your knowledge hub WIEN

Path following control in a collaborative task is covered in [11]. The separately controllable tangential and transversal motion is exploited to vary the robot behavior while moving along the path. By coupling the control parameters to the path progress a varying stiffness along certain sections is implemented. Using various settings for the path progression different cooperation modes are presented. The findings are evaluated using a KUKA *iiwa* robot in an assembly task.

The work of [12] uses kinesthetic programming for robotic rope-winding. A motor with a rope on a spool, mounted on the flange of a KUKA LWR4+, is manually guided around obstacles while points along the desired path are recorded. A quartic spline is created which resembles the guided curve. PFC with feedback linearization is used to control the robot motion. The desired end-effector orientation is calculated from the defined path. Additionally, this work compares the Frenet-Serret frame with the PT frame for this purpose. During reenactment the rope tension is controlled to be constant.

1.2 Structure of this Thesis

This thesis describes the design and implementation of a force sensitive teach-in process demonstrated on a rope-winding scenario.

Before presenting the designed tool, the control strategy and implementation, the model of the used KUKA LBR iiwa 14 R820 robot is derived in Chapter 2. A kinematic model of the robot is obtained in Section 2.1. Subsequently, a dynamic model, incorporating the joint elasticity, results from the Euler-Lagrange equations in Section 2.3.

The designed manual teach-in tool is introduced in Chapter 3. The sensor selection is described along with the design requirements and the final design.

The path following control strategy is discussed in Chapter 4. First, the properties of the PT frame are outlined and the control objectives are defined. Second, the feedback transformation is shown in Section 4.4 and the extension of the null space in Section 4.3. Finally, the control law is presented.

In Chapter 5, the implementation and results are described. The path recording and post-processing is outlined in Section 5.1. The following sections present the simulation and experimental results of this work.

Die approbierte gedruckte Originalversion dieser Diplomarbeit ist an der TU Wien Bibliothek verfügbar.
The approved original version of this thesis is available in print at TU Wien Bibliothek.
TU Bibliothek Your knowledge hub WIEN

2 Mathematical Modeling

In this chapter, the necessary steps to derive a mathematical model of the used *KUKA iiwa* robot are outlined. With the obtained model, the dynamic behavior of the robot can be described, which serves as a basis for the controller design.

First, the computation of the forward kinematic model is described using homogeneous transformations and the Denavid-Hartenberg (DH) convention. This describes the end-effector position and orientation as a function of the joint angles.

Second, using the kinematic relations the manipulator Jacobian is derived. This matrix maps the joint velocities to the velocities of the task space and is used in the third part to compute the equations of motion with the Euler-Lagrange formalism. The described steps can be found in [13, 14].

Since the *KUKA iiwa* is a collaborative robot designed for human-robot interaction, its joints are not inherently stiff, which needs to be considered in the equations of motion. Based on [15], a reduced model is derived. Using the singular perturbation approach, the dynamics of the system are split into a fast and slow part and controlled in a cascaded structure.

2.1 Kinematic Model

The forward kinematics of the robot describes the end-effector pose as a function of the joint angles. Homogeneous transformations are used to compute the forward kinematic model. This transformation describes the relation of orientation and position between two coordinate systems (CS) and is assembled in the form

$$\mathbf{T} = \begin{bmatrix} \mathbf{R}_{3\times3} & \mathbf{p}_{3\times1} \\ \mathbf{0}_{1\times3} & 1_{1\times1} \end{bmatrix}. \tag{2.1}$$

It comprises a rotation matrix $\mathbf{R}$ and a translation vector $\mathbf{p}$. Since the robot is modeled as a series of connected rigid bodies, homogeneous transformation matrices are used to describe the relation of each successive link to its former link. Multiplication of these successive transformations leads to the forward kinematic model of the robot. The DH convention provides guidelines for the assignment of a CS to each link. Based on the assigned CS the homogeneous transformation for each link is systematically assembled. Figure 2.1 shows an image of the KUKA *iiwa* with the assigned CS. The corresponding DH parameters are listed in Table 2.1.

As stated in Chapter 1, the motor on the end-effector is tilted to enable more advantageous configurations of the robot for the task at hand. The tilt is considered by

Die approbierte gedruckte Originalversion dieser Diplomarbeit ist an der TU Wien Bibliothek verfügbar.
The approved original version of this thesis is available in print at TU Wien Bibliothek.

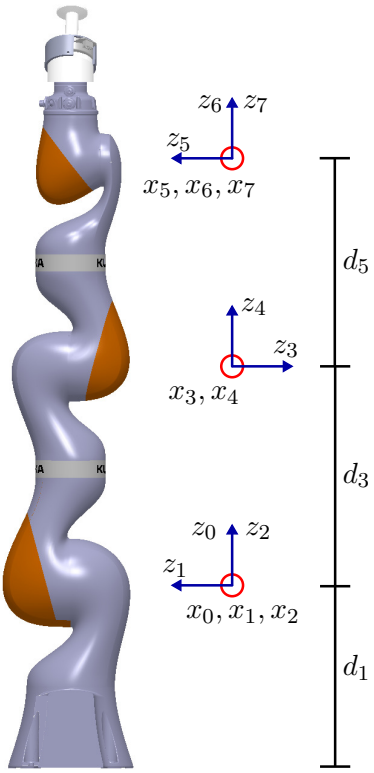

Figure 2.1: KUKA *iiwa* with assinged CS for the links.

Link	θ_i	d_i	a_i	α_i
1	q_1	d_1	0	$\frac{\pi}{2}$
2	q_2	0	0	$-\frac{\pi}{2}$
3	q_3	d_3	0	$-\frac{\pi}{2}$
4	q_4	0	0	$\frac{\pi}{2}$
5	q_5	d_5	0	$\frac{\pi}{2}$
6	q_6	0	0	$-\frac{\pi}{2}$
7	q_7	0	0	0

Table 2.1: DH parameters for each link.

introducing an additional transformation for the *tool center point* (TCP) according to

$$\mathbf{T}_7^{tcp} = \begin{bmatrix} \cos\alpha & 0 & -\sin\alpha & 0 \\ 0 & 1 & 0 & 0 \\ \sin\alpha & 0 & \cos\alpha & l_t \\ 0 & 0 & 0 & 1 \end{bmatrix}, \tag{2.2}$$

describing the tilt angle α about the y-axis of the tool frame and the offset along the z-axis l_t.

Die approbierte gedruckte Originalversion dieser Diplomarbeit ist an der TU Wien Bibliothek verfügbar.
The approved original version of this thesis is available in print at TU Wien Bibliothek.
TU Bibliothek Your knowledge hub WIEN

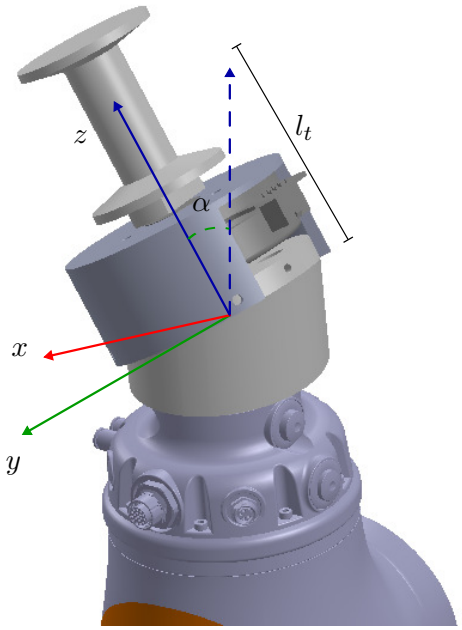

Figure 2.2: Tilted motor with the spool on the end-effector of the robot.

Finally, the kinematic description is assembled by multiplying the transformation matrices of each link, resulting in

$$\mathbf{T}_0^{tcp}(\mathbf{q}) = \mathbf{T}_0^1\mathbf{T}_1^2\mathbf{T}_2^3\mathbf{T}_3^4\mathbf{T}_4^5\mathbf{T}_5^6\mathbf{T}_6^7\mathbf{T}_7^{tcp}, \tag{2.3}$$

with $\mathbf{q}$ denoting the current joint configuration. The used robot parameters for the kinematic description are listed in Appendix A.1.1.

2.2 Differential Kinematics

The relation of the joint velocities and the linear and angular velocities of the links are described by the manipulator Jacobian matrix. Utilizing this matrix to map between joint and task space is referred to as differential kinematics. To obtain the manipulator Jacobian the position vector to the center of mass $\mathbf{p}_0^i$ for each link is used. The partial derivative of $\mathbf{p}_0^i$ with respect to $\mathbf{q}$ yields

$$\mathbf{v}_0^i = \mathbf{J}_{v_i}(\mathbf{q})\dot{\mathbf{q}}, \tag{2.4}$$

which relates the joint velocities to the linear velocities of link i, with

$$\mathbf{J}_{v_i}(\mathbf{q}) = \left[\frac{\partial \mathbf{p}_0^i}{\partial q_1}(\mathbf{q}), \ldots, \frac{\partial \mathbf{p}_0^i}{\partial q_n}(\mathbf{q})\right]. \tag{2.5}$$

The vector $\boldsymbol{\omega}_0^i$, describing the angular velocity about axis i, is utilized to compute the rotational part of the Jacobian matrix according to

$$\mathbf{J}_{\omega_i}(\mathbf{q}) = \left[\frac{\partial \boldsymbol{\omega}_0^i}{\partial q_1}(\mathbf{q}), \ldots, \frac{\partial \boldsymbol{\omega}_0^i}{\partial q_n}(\mathbf{q})\right]. \tag{2.6}$$

Die approbierte gedruckte Originalversion dieser Diplomarbeit ist an der TU Wien Bibliothek verfügbar.
The approved original version of this thesis is available in print at TU Wien Bibliothek.
TU Bibliothek Your knowledge hub WIEN

The angular velocity vector $\boldsymbol{\omega}_0^i(\mathbf{q})$ can be calculated from the skew-symmetric matrix

$$\mathbf{S}(\boldsymbol{\omega}_0^i) = \dot{\mathbf{R}}_0^i(\mathbf{R}_0^i)^{\mathrm{T}} = \begin{bmatrix} 0 & -\omega_z & \omega_z \\ \omega_z & 0 & -\omega_x \\ -\omega_y & \omega_x & 0 \end{bmatrix}, \tag{2.7}$$

which contains the angular velocities around each respective axis. The matrix $\mathbf{R}_0^i$ describes the rotation of link i with $\dot{\mathbf{R}}_0^i$ denoting the time derivative of the rotation matrix. Equations (2.5) and (2.6) are assembled into the manipulator Jacobian matrix

$$\mathbf{J}_0^i(\mathbf{q}) = \begin{bmatrix} \mathbf{J}_{v_i}(\mathbf{q}) \\ \mathbf{J}_{\omega_i}(\mathbf{q}) \end{bmatrix}_{6\times 7}. \tag{2.8}$$

Note that $\mathbf{J}_0^i$ is of dimension $\mathbb{R}^{6\times 7}$ since the robot has 7 degrees of freedom (DOF) corresponding to the 7 joints. The task space is of dimension 6, 3 translational and 3 rotational DOF. This additional dimension is the so called null space of the robot which allows the movement of the arm while fixing the end-effector pose. The computed manipulator Jacobian matrices provide the mapping of the joint velocities to the velocities of the task space

$$\begin{bmatrix} \mathbf{v}_0^i \\ \boldsymbol{\omega}_0^i \end{bmatrix} = \mathbf{J}_0^i(\mathbf{q})\dot{\mathbf{q}}. \tag{2.9}$$

2.3 Dynamic Model

The dynamical model of the robot, consisting of $n = 7$ connected rigid bodies, is derived using the Euler-Lagrange equations, expressed by

$$\frac{\mathrm{d}}{\mathrm{d}t}\left(\frac{\partial \mathcal{L}}{\partial \dot{\mathbf{q}}}\right)^{\mathrm{T}} - \left(\frac{\partial \mathcal{L}}{\partial \mathbf{q}}\right)^{\mathrm{T}} = \boldsymbol{\tau}. \tag{2.10}$$

These equations establish the relation between the applied generalized torques $\boldsymbol{\tau}$ and the motion of the robot. The expressions $\mathbf{q}$ and $\dot{\mathbf{q}}$ in (2.10) refer to the generalized coordinates and generalized velocities, respectively. The Lagrangian function

$$\mathcal{L} = \mathcal{T} - \mathcal{V} \tag{2.11}$$

consists of the difference between the kinetic energy $\mathcal{T}$ and the potential energy $\mathcal{V}$ of the system.

The kinetic energy of the system is described by

$$\mathcal{T} = \frac{1}{2}\sum_{i=0}^{n}\Big(m_i(\mathbf{v}_0^i)^{\mathrm{T}}\mathbf{v}_0^i + (\boldsymbol{\omega}_0^i)^{\mathrm{T}}(\mathbf{R}_0^i)^{\mathrm{T}}\boldsymbol{\Theta}_i^i(\mathbf{R}_0^i)\boldsymbol{\omega}_0^i\Big), \tag{2.12}$$

with the mass m_i and the inertia matrix $(\mathbf{R}_0^i)^{\mathrm{T}}\boldsymbol{\Theta}_i^i(\mathbf{R}_0^i)$ of the respective link i, expressed in the inertial frame referred to with the index 0. Note that $\boldsymbol{\Theta}_i^i$ is the inertia matrix expressed in the link-fixed coordinate frame. The linear and angular velocities $(\mathbf{v}_0^i, \boldsymbol{\omega}_0^i)$ of

Die approbierte gedruckte Originalversion dieser Diplomarbeit ist an der TU Wien Bibliothek verfügbar.
The approved original version of this thesis is available in print at TU Wien Bibliothek.
TU Bibliothek Your knowledge hub WIEN

each link are expressed using the respective manipulator Jacobian matrices, derived in Section 2.2. Insertion of (2.9) into (2.12) yields

$$\mathcal{T} = \frac{1}{2}\dot{\mathbf{q}}^{\mathrm{T}} \underbrace{\sum_{i=1}^{n} \Big[m_i (\mathbf{J}_{v_i})^{\mathrm{T}}(\mathbf{q}) \mathbf{J}_{v_i}(\mathbf{q}) + (\mathbf{J}_{\omega_i})^{\mathrm{T}}(\mathbf{q}) (\mathbf{R}_0^i)^{\mathrm{T}} \boldsymbol{\Theta}_i^i \mathbf{R}_0^i \mathbf{J}_{\omega_i}(\mathbf{q}) \Big]}_{\mathbf{M}(\mathbf{q})} \dot{\mathbf{q}}. \tag{2.13}$$

Therein, $\mathbf{M}(\mathbf{q})$ is the mass matrix of the system.

The potential energy of the system is due to the gravitational force

$$\mathcal{V}(\mathbf{q}) = \sum_{i=0}^{n} m_i \begin{bmatrix} 0 & 0 & g \end{bmatrix} \mathbf{p}_0^i(\mathbf{q}), \tag{2.14}$$

with g acting in the negative z-direction.

The partial derivative of this expression yields

$$\mathbf{g}(\mathbf{q}) = \frac{\partial \mathcal{V}(\mathbf{q})}{\partial \mathbf{q}}, \tag{2.15}$$

which represents the vector of potential forces.

Inserting the obtained expressions for the kinetic and potential energy into the Euler-Lagrange equations (2.10), the equations of motion for the robot system result in

$$\mathbf{M}(\mathbf{q})\ddot{\mathbf{q}} + \mathbf{C}(\mathbf{q}, \dot{\mathbf{q}})\dot{\mathbf{q}} + \mathbf{g}(\mathbf{q}) = \boldsymbol{\tau}. \tag{2.16}$$

The matrix $\mathbf{C}(\mathbf{q}, \dot{\mathbf{q}})$ represents the Coriolis and centrifugal forces while $\boldsymbol{\tau}_{ext}$ denotes the generalized forces (external torques and forces, dissipative torques and forces). The elements of the Coriolis matrix are assembled according to

$$\mathbf{C}(\mathbf{q}, \dot{\mathbf{q}})[k, j] = \sum_{i=1}^{n} c_{ijk}(\mathbf{q}) \dot{q}_i, \tag{2.17}$$

with $c_{ijk}(\mathbf{q})$ denoting the Christoffel symbols of the first kind, which are computed using the elements $m_{ij} = \mathbf{M}_{[i,j]}$ of the mass matrix

$$c_{ijk} = \frac{1}{2}\left(\frac{\partial m_{kj}(\mathbf{q})}{\partial q_i} + \frac{\partial m_{ki}(\mathbf{q})}{\partial q_j} - \frac{\partial m_{ij}(\mathbf{q})}{\partial q_k} \right). \tag{2.18}$$

To consider the joint elasticity of the robot the equations of motion (2.16) are modified according to [15]. Using this method, the system can be split in a fast and slow subsystem. The fast subsystem considers the elasticity in the joints whereas the slow subsystem represents the rigid-body structure. A cascaded controller is used with an inner loop that stabilizes the desired torque of the outer loop. After the application of this method the resulting model takes the form

$$\underbrace{\left(\mathbf{M}(\mathbf{q}) + (\mathbf{I} + \mathbf{K}_\tau)^{-1}\mathbf{B}\right)}_{\tilde{\mathbf{M}}(\mathbf{q})} \ddot{\mathbf{q}} + \mathbf{C}(\mathbf{q}, \dot{\mathbf{q}})\dot{\mathbf{q}} + \mathbf{g}(\mathbf{q}) = \boldsymbol{\tau}. \tag{2.19}$$

Die approbierte gedruckte Originalversion dieser Diplomarbeit ist an der TU Wien Bibliothek verfügbar.
The approved original version of this thesis is available in print at TU Wien Bibliothek.
TU Bibliothek Your knowledge hub WIEN

As can be seen, only the mass matrix of the system needs to be modified to account for the elasticity of the joints of the robot. The expressions $\mathbf{I}$, $\mathbf{K}_\tau$ and $\mathbf{B}$ in (2.19) denote the identity matrix, the controller gain of the underlying singular perturbation controller and the moments of inertia of the motors, respectively. The values for the described matrices are listed in Appendix A.1.5.

Die approbierte gedruckte Originalversion dieser Diplomarbeit ist an der TU Wien Bibliothek verfügbar.
The approved original version of this thesis is available in print at TU Wien Bibliothek.
TU Bibliothek Your knowledge hub WIEN

3 Teach-In Tool

To facilitate the teach-in process, where a rope has to be wound with a desired force, a manual teach-in tool is introduced that enables the intuitive demonstration of this task. This chapter describes the designed teach-in tool and the involved sensors.

In the first part, the design requirements for the tool are outlined. After the used sensors are described in more detail in the second part, the tool design is presented.

3.1 Requirements

The concept of force teach-in is evaluated by a rope-winding task, which is set up using a spool with a rope on the flange of the robot. To enable an intuitive demonstration of the task a similar spool is integrated into the teach-in tool to facilitate the mapping between the teach-in and the application of the recorded trajectory to the robot (reenactment).

To demonstrate a path during teach-in the position of the tool must be tracked. The measured pose needs to be related to the position of the robot and combined with the force information resulting from the rope tension. Therefore, a combined pose and force measurement needs to be implemented.

Apart from these considerations, when designing the tool, emphasis was placed on handiness and robustness. Since the recording of paths should be possible in different scenarios, the tool needs to be compact in size but also lightweight to facilitate single-handed use of the operator. In addition, the tool should be robust to withstand the tension forces when stretching the rope and hence provide tactile feedback during teach-in.

3.2 Sensor Selection

Depending on the design, the acceleration of the spool can be a problem. If a force/torque sensor is utilized additional forces and torques due to bending, gravity and motion is measured. A rotary torque sensor, on the other hand, can only measure the torque acting on its axis. This can lead to errors during the measurement if the applied torque does not act perpendicular to the sensor axis. However, these errors due to misalignment are considered negligible. During reenactment the spool orientation is controlled to be orthogonal to the rope.

To measure the applied tension force that acts on the rope while unwinding the rope and recording the path, a rotary torque sensor is used. The spool is mounted on one side of the torque sensor which requires a breaking mechanism on the opposite side to twist the shaft of the sensor. The measured torque is proportional to the torsion on the shaft. The selected sensor has a measurement range of $0 \ldots 2\,\mathrm{N\,m}$ which corresponds to a pulling

Die approbierte gedruckte Originalversion dieser Diplomarbeit ist an der TU Wien Bibliothek verfügbar.
The approved original version of this thesis is available in print at TU Wien Bibliothek.
TU Bibliothek Your knowledge hub WIEN

force, considering the used spool diameter $d_s = 24.6\,\text{mm}$, of approximately

$$F_r = \frac{2\,\text{N m}}{\frac{d_{spool}}{2}} \approx 162.6\,\text{N}. \tag{3.1}$$

This measurement range complies with the requirements stated above, assuring that the tool can be built to handle the pulling forces applied by an operator. Furthermore, the motor mounted on the end-effector of the robot has a nominal torque of 560 mN m (see Appendix A.1.2). This means that the motor is not able to reproduce the full torque range of the sensor during reenactment. A torque sensor from ETH-Messtechnik [16], depicted in Figure 3.1, is used. The technical specifications of the sensor are listed in Appendix A.1.3.

Figure 3.1: Rotary torque sensor used in the teach-in tool.

An Optitrack [17] camera system is utilized for the tracking of the pose of the tool during teach-in, using the *Prime 17W* cameras. This system uses infrared tracking markers that need to be placed on the tool and are recorded by the cameras. With a measurement accuracy up to sub-millimeter range and an adjustable frame rate of up to 360 frames per second (FPS) this system provides an ideal means for tracking the pose of the teach-in tool in the 3D space. On the tool, a mounting point to attach a marker body, a so called *hand rigid-body marker set*, needs to be considered. The marker body, used for tracking, is depicted in Figure 3.2 with the markers mounted on the ends.

3.3 Tool Design

The final tool design used for the measurements and evaluations is depicted in Figure 3.3. In order to facilitate the design process, the parts for the tool where manufactured using a 3D printer. This enables the construction of a lightweight, albeit robust teach-in tool.

By applying a breaking force and pulling the rope during teach-in the shaft of the torque sensor is twisted which results in a measurable torque. To track the pose of the tool in the 3D space the maker body, shown in Figure 3.2, is mounted at the front side. The CS is located at the geometric center of mounted markers. Since the marker arrangement is asymmetrical, the distinct orientation of the tool can be obtained.

Die approbierte gedruckte Originalversion dieser Diplomarbeit ist an der TU Wien Bibliothek verfügbar.
The approved original version of this thesis is available in print at TU Wien Bibliothek.
TU Bibliothek Your knowledge hub WIEN

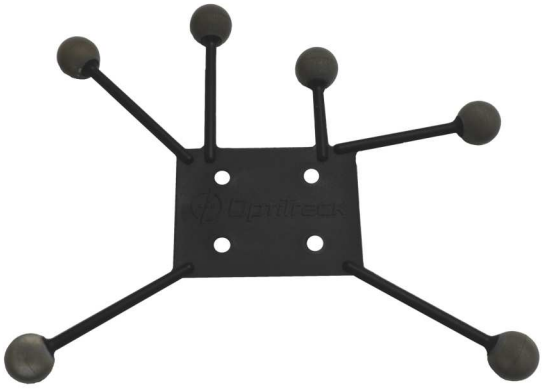

Figure 3.2: Marker body with infrared markers. This body is mounted on the teach-in tool for tracking the pose.

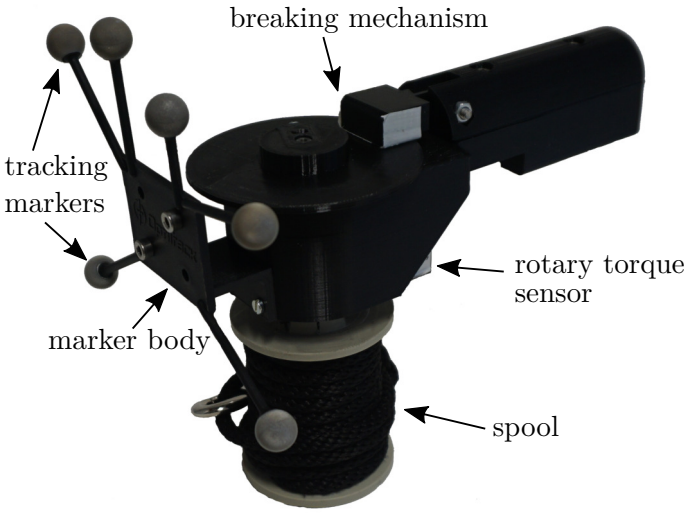

Figure 3.3: Designed manual teach-in tool.

The torque sensor is integrated into the tool. The spool with the rope is mounted on the torque sensor at one side and is protruding. This provides easier rope handling and facilitates the teach-in process. On the top side of the sensor, a breaking mechanism is implemented for the stretching of the rope.

The recorded position, corresponding to the geometric center of the optical markers, is converted to the center of the spool using the transformation

$$\mathbf{T}_r^s = \begin{bmatrix} 1 & 0 & 0 & d_x \\ 0 & 1 & 0 & d_y \\ 0 & 0 & 1 & d_z \\ 0 & 0 & 0 & 1 \end{bmatrix}. \tag{3.2}$$

Die approbierte gedruckte Originalversion dieser Diplomarbeit ist an der TU Wien Bibliothek verfügbar.
The approved original version of this thesis is available in print at TU Wien Bibliothek.
TU Bibliothek Your knowledge hub WIEN

Thus, a description of the path of the spool is obtained. The expressions $d_{\{x,y,z\}}$ denote the distances in the respective directions to the spool center point. The values for the used distances are listed in Appendix A.1.4. Figure 3.4 shows the CS of the tool with Σ_r and Σ_s for the marker body and spool CS, respectively. Note that the z-axis is pointing downwards. In the course of this work, the z-axis of the tool represents the spool vector, which is a determining variable for the path following controller.

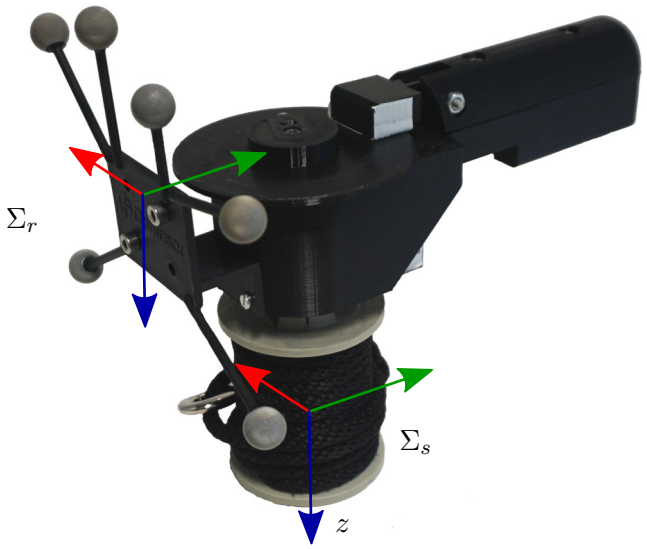

Figure 3.4: Teach-in tool with marker body and spool CS.

Die approbierte gedruckte Originalversion dieser Diplomarbeit ist an der TU Wien Bibliothek verfügbar.
The approved original version of this thesis is available in print at TU Wien Bibliothek.
TU Bibliothek Your knowledge hub WIEN

4 Path Following Control

To control the motion of the robot along a given curve, a path following control (PFC) is implemented. As in [10] and [11] the parallel transport (PT) frame is used to construct an orthonormal frame at every point of the parametrized path. Based on this frame, a PFC is implemented to control the tangential, transversal and rotational motion of the end-effector separately.

First, the control objectives, with respect to the position and orientation of the end-effector of the robot and the requirements concerning the properties of the path are introduced. In the following section, the construction of the PT frame from a given parametrized path is described.

Second, the modification of the null space of the robot is discussed. The spool mounted on the end-effector is a rotationally symmetric body. Hence controlling the rotation around the z-axis of the end-effector, i. e. the spool axis, does not provide any functional benefit. This circumstance is utilized in this work to improve the path following by transferring this rotational degree of freedom (DOF) to the null space of the robot. This results in a reduced task space of five DOF, three for the end-effector position in space and two for the end-effector orientation. The remaining two DOF are then used to enhance the dexterity of the robot and facilitate the teach-in process.

Finally, to define the control objectives relative to the path a feedback linearization is used. This establishes a linear relation between the input and the output of the system to which a compliance controller is applied to impose the desired behavior.

4.1 Problem Statement

The objective of the PFC is to move the tool center point (TCP) of the robot, in this case the spool, along a given path γ while compensating for external forces, e.g. the pulling force of the unwinding rope. This section outlines the control objectives as well as the required properties of the path γ.

The position $\mathbf{y}_t$ and orientation $\mathbf{y}_r$ of the end-effector form the output of the system to be controlled,

$$\mathbf{y} = \begin{bmatrix} \mathbf{y}_t \\ \mathbf{y}_r \end{bmatrix} = \begin{bmatrix} \mathbf{h}_t(\mathbf{q}) \\ \mathbf{h}_r(\mathbf{q}) \end{bmatrix} = \mathbf{h}(\mathbf{q}), \tag{4.1}$$

with $\mathbf{h}(\mathbf{q})$ describing the forward kinematics. The derivative with respect to time of (4.1), with the Jacobian matrix $\mathbf{J}(\mathbf{q})$ according to (2.9), yields

$$\dot{\mathbf{y}} = \begin{bmatrix} \dot{\mathbf{y}}_t \\ \dot{\mathbf{y}}_r \end{bmatrix} = \underbrace{\begin{bmatrix} \mathbf{J}_t(\mathbf{q}) \\ \mathbf{J}_r(\mathbf{q}) \end{bmatrix}}_{\mathbf{J}(\mathbf{q})} \dot{\mathbf{q}}. \tag{4.2}$$

Die approbierte gedruckte Originalversion dieser Diplomarbeit ist an der TU Wien Bibliothek verfügbar.
The approved original version of this thesis is available in print at TU Wien Bibliothek.
TU Bibliothek Your knowledge hub WIEN

A parameterized curve $\boldsymbol{\sigma}^{\mathrm{T}}(\theta)$ of a path γ is given with the path progress parameter θ. The curve contains a translational and rotational part, i.e. $\boldsymbol{\sigma}^{\mathrm{T}}(\theta) = \begin{bmatrix}\boldsymbol{\sigma}_t^{\mathrm{T}}(\theta) & \boldsymbol{\sigma}_r^{\mathrm{T}}(\theta)\end{bmatrix} : \mathcal{T} \mapsto \mathbb{R}^6$. For fully actuated robots the parameterized curve needs to be threefold continuously differentiable (i.e. C^3) and regular, see [18]. This means the tangential vector must not become zero,

$$\boldsymbol{\sigma}_t'(\bar{\theta}) = \left(\frac{\partial \boldsymbol{\sigma}_t}{\partial \theta}\right)(\bar{\theta}) \neq \mathbf{0}, \tag{4.3}$$

for any $\bar{\theta}$.

For the definition of the control objectives, the shortest distance to the path γ_t is used, i. e. $\|\mathbf{y}_t\|_{\gamma_t} = \inf_{\bar{\mathbf{y}}_t \in \gamma_t} \|\mathbf{y}_t - \bar{\mathbf{y}}_t\|_2$. As outlined in [10], the control objectives are defined as follows:

($\mathcal{O}1$) Asymptotic convergence to $\boldsymbol{\sigma}_t(\theta)$: $\mathbf{y}_t$, the end-effector position, converges to the path, $\|\mathbf{y}_t(t)\|_{\gamma_t} \to 0$ for $t \to \infty$.

($\mathcal{O}2$) Invariance property: If the position and velocity of the system output at t_0, i. e.. $[\mathbf{q}(t_0)^{\mathrm{T}} \quad \dot{\mathbf{q}}(t_0)^{\mathrm{T}}]^{\mathrm{T}}$, are elements of $\Gamma^* \subset \Gamma$, $\Gamma = \{[\mathbf{q}^{\mathrm{T}} \quad \dot{\mathbf{q}}^{\mathrm{T}}]^{\mathrm{T}} \in \mathbb{R}^{14} : \mathbf{h}(\mathbf{q}) \in \gamma\}$, then $\|\mathbf{y}_t(t)\|_{\gamma_t} = 0$, $\forall t \geq t_0$.

($\mathcal{O}3$) Tangential motion: The motion on the path can be adjusted according to desired specifications e.g. speed or direction of traversal.

4.2 Path Coordinate System

In this section, the PT frame is used to construct an orthonormal frame at every point of the parametrized curve $\boldsymbol{\sigma}(\theta)$. This frame has the advantage, in contrast to the Frenet-Serret frame, see [18], that it is also defined on path segments where the curvature is zero, e. g. straight lines. The usage of such a frame allows to construct a local coordinate system (CS) where task coordinates relative to the path can be defined. The unit vectors of the resulting frame are used to obtain a coordinate transformation from the system output $\mathbf{y} = \begin{bmatrix}\mathbf{y}_t^{\mathrm{T}} & \mathbf{y}_r^{\mathrm{T}}\end{bmatrix}^{\mathrm{T}}$ to the virtual output $\hat{\mathbf{y}} = \begin{bmatrix}\hat{\mathbf{y}}_t^{\mathrm{T}} & \hat{\mathbf{y}}_r^{\mathrm{T}}\end{bmatrix}^{\mathrm{T}}$.

Note that here variables with a hat, e. g. $\hat{\mathbf{x}}$, refer to the virtual output. These variables are expressed in a local CS on the path. For the modified null space, which is to be described in the following, a tilde symbol is utilized, e. g. $\tilde{\mathbf{x}}$.

Figure 4.1 shows the CS on the path with the relevant parameters. The tangential, normal and orthonormal unit vectors of the PT frame are denoted by $\mathbf{e}_i(\theta)$, with $i = \{1, 2, 3\}$, respectively. The expression η represents the new tangential coordinate whereas ξ_1 and ξ_2 are the new transversal coordinates. The current tangential unit vector is calculated in the form

$$\mathbf{e}_1(\theta) = \frac{\boldsymbol{\sigma}_t'(\theta)}{\|\boldsymbol{\sigma}_t'(\theta)\|_2}. \tag{4.4}$$

Due to the regularity of the provided curve being ensured by the assumptions in (4.3), $\mathbf{e}_1(\theta)$ is always defined. The orthonormal CS results from the system of differential-algebraic

Die approbierte gedruckte Originalversion dieser Diplomarbeit ist an der TU Wien Bibliothek verfügbar.
The approved original version of this thesis is available in print at TU Wien Bibliothek.
TU Bibliothek Your knowledge hub WIEN

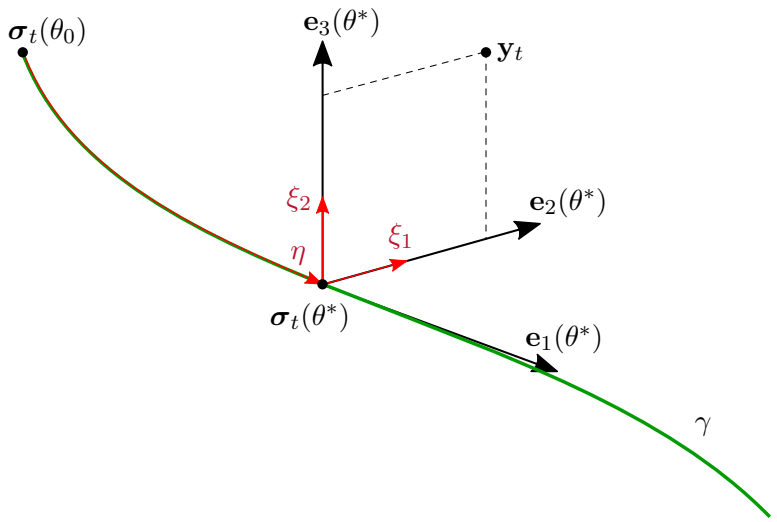

Figure 4.1: PT frame on a path γ.

equations

$$\mathbf{e}_i'(\theta) = \gamma_i(\theta)\mathbf{e}_1(\theta), \quad \mathbf{e}_i(\theta_0) = \mathbf{e}_{i,0} \tag{4.5a}$$

$$0 = 1 - \mathbf{e}_i^{\mathrm{T}}(\theta)\mathbf{e}_i(\theta) \tag{4.5b}$$

$$0 = \mathbf{e}_1^{\mathrm{T}}(\theta)\mathbf{e}_i(\theta), \tag{4.5c}$$

see [10], with $i \in \{2, 3\}$ denoting the normal and orthonormal coordinates of the frame. These equations ensure that the time derivative of the normal and orthonormal vector points in the direction of the tangential vector. The resulting vectors are normalized and form an orthonormal basis, see [19]. While $\mathbf{e}_2(\theta)$ is calculated from (4.4) and (4.5), $\mathbf{e}_3(\theta)$ can be obtained from

$$\mathbf{e}_3(\theta) = \mathbf{e}_1(\theta) \times \mathbf{e}_2(\theta). \tag{4.6}$$

Position on the Path

During operation the closest point of the TCP on the path is computed. This position is determined by solving an optimization problem at every time step, which is given by

$$\theta^* = \mathrm{P}_{\mathcal{T}}(\mathbf{y}_t) = \arg\min_{\theta \in \mathcal{T}} \|\mathbf{y}_t - \boldsymbol{\sigma}_t(\theta)\|_2^2, \tag{4.7}$$

with the projection operator $\mathrm{P}_{\mathcal{T}}(\mathbf{y}_t)$ denoting the orthogonal projection of the TCP, i. e. $\mathbf{y}_t$, on the path $\boldsymbol{\sigma}_t(\theta)$. As outlined in [10], if the optimal path parameter θ^* is an interior point of $\mathcal{T} \subseteq \mathbb{R}$, the first-order necessary condition for optimality is satisfied. From the second-order sufficient condition for optimality the new parameter $\alpha(\mathbf{y}_t)$ is introduced,

$$\alpha(\mathbf{y}_t) = \frac{(\mathbf{y}_t - \boldsymbol{\sigma}_t(\theta^*))^{\mathrm{T}} \boldsymbol{\sigma}_t''(\theta^*)}{\|\boldsymbol{\sigma}_t'(\theta^*)\|_2^2}. \tag{4.8}$$

Die approbierte gedruckte Originalversion dieser Diplomarbeit ist an der TU Wien Bibliothek verfügbar.
The approved original version of this thesis is available in print at TU Wien Bibliothek.
TU Bibliothek Your knowledge hub WIEN

This allows to define a feasible neighborhood of the path according to $\gamma_t = \{\mathbf{y}_t \in \mathbb{R}^3 : \alpha(\mathbf{y}_t) < 1\}$ where the optimization problem (4.7) is well defined and a strict minimum exists.

Tangential and Transversal Subsystem

The newly defined coordinates η, ξ_1 and ξ_2 are assembled to form the new output,

$$\hat{\mathbf{y}}_t = \begin{bmatrix} \eta \\ \xi_1 \\ \xi_2 \end{bmatrix}, \tag{4.9}$$

with η denoting the tangential and $\xi_{\{1,2\}}$ the transversal subsystem, respectively. The coordinate η is defined as the arc length along the path,

$$\eta = \int_{\theta_0}^{\theta^*} \left\| \boldsymbol{\sigma}_t'(\tau) \right\|_2 d\tau, \tag{4.10}$$

with the derivative with respect to time

$$\dot{\eta} = \left\| \boldsymbol{\sigma}_t'(\theta^*) \right\|_2 \dot{\theta}^* = \beta(\mathbf{y}_t) \mathbf{e}_1^{\mathrm{T}}(\theta^*) \dot{\mathbf{y}}_t, \tag{4.11}$$

and the auxiliary parameter $\beta(\mathbf{y}_t) = \frac{1}{1-\alpha(\mathbf{y}_t)}$.

The transversal subsystem is obtained by projection of the distance vector onto the respective vectors of the transversal subsystem of the frame, as shown in Figure 4.1. The transformation is done for the transversal coordinates according to

$$\xi_1 = \mathbf{e}_2^{\mathrm{T}}(\theta^*)(\mathbf{y}_t - \boldsymbol{\sigma}_t(\theta^*)), \tag{4.12}$$

$$\xi_2 = \mathbf{e}_3^{\mathrm{T}}(\theta^*)(\mathbf{y}_t - \boldsymbol{\sigma}_t(\theta^*)), \tag{4.13}$$

with the respective time derivatives

$$\dot{\xi}_1 = \mathbf{e}_2^{\mathrm{T}}(\theta^*) \dot{\mathbf{y}}_t, \tag{4.14}$$

$$\dot{\xi}_2 = \mathbf{e}_3^{\mathrm{T}}(\theta^*) \dot{\mathbf{y}}_t. \tag{4.15}$$

Rotational Subsystem

The rotational subsystem is used to describe the orientation of the end-effector, in this case the spool. This orientation is formally described by $\boldsymbol{\zeta}_r$ relative to the base CS in the form

$$\boldsymbol{\zeta}_r = \mathbf{y}_r = \mathbf{h}_r(\mathbf{q}), \tag{4.16}$$

with the time derivative

$$\dot{\boldsymbol{\zeta}}_r = \dot{\mathbf{y}}_r = \mathbf{J}_r(\mathbf{q}) \dot{\mathbf{q}}. \tag{4.17}$$

The rotational part of the end-effector Jacobian matrix is represented by $\mathbf{J}_r(\mathbf{q})$, see (4.2).

During the teach-in phase the orientation of the tool is measured and $\mathbf{R}_0^s(\theta^*)$ describes the orientation of the spool mounted on the teach-in tool relative to the base CS. Note that

Die approbierte gedruckte Originalversion dieser Diplomarbeit ist an der TU Wien Bibliothek verfügbar.
The approved original version of this thesis is available in print at TU Wien Bibliothek.
TU Bibliothek Your knowledge hub WIEN

this orientation depends on the position θ^* along the path. For the rotational subsystem, the angular velocity $\dot{\boldsymbol{\zeta}}_r$ of (4.17) is transformed relative to the orientation during the teach-in phase at every position θ^* along the path in the form

$$\dot{\boldsymbol{\zeta}}_r^{\Delta} = (\mathbf{R}_0^s(\theta^*))^{\mathrm{T}} \mathbf{J}_r(\mathbf{q})\dot{\mathbf{q}}. \tag{4.18}$$

Henceforth, $\boldsymbol{\zeta}_r^{\Delta}$ formally describes the orientation related to (4.18).

Definition of the Virtual Output

The output of the system $\begin{bmatrix}\mathbf{y}^{\mathrm{T}} & \dot{\mathbf{y}}^{\mathrm{T}}\end{bmatrix}^{\mathrm{T}}$, as described by (4.1) and (4.2), denotes the position and orientation of the spool in the base CS of the robot. The virtual output $\begin{bmatrix}\hat{\mathbf{y}}^{\mathrm{T}} & \dot{\hat{\mathbf{y}}}^{\mathrm{T}}\end{bmatrix}^{\mathrm{T}}$ is formed using the previously described subsystems. The composition of the tangential, transversal and rotational subsystem yields

$$\hat{\mathbf{y}} = \begin{bmatrix} \eta \\ \xi_1 \\ \xi_2 \\ \boldsymbol{\zeta}_r^{\Delta} \end{bmatrix}, \tag{4.19}$$

which describes the position of the spool in the local CS, i. e. the PT frame, whereas the spool orientation is expressed in the reference frame. The time derivative of (4.19) yields

$$\dot{\hat{\mathbf{y}}} = \begin{bmatrix} \dot{\hat{\mathbf{y}}}_t \\ \dot{\hat{\mathbf{y}}}_r \end{bmatrix} = \begin{bmatrix} \dot{\eta} \\ \dot{\xi}_1 \\ \dot{\xi}_2 \\ \dot{\boldsymbol{\zeta}}_r^{\Delta} \end{bmatrix} = \underbrace{\begin{bmatrix} \beta(\mathbf{y}_t)\mathbf{e}_1^{\mathrm{T}}(\theta^*) & \mathbf{0} \\ \mathbf{e}_2^{\mathrm{T}}(\theta^*) & \mathbf{0} \\ \mathbf{e}_3^{\mathrm{T}}(\theta^*) & \mathbf{0} \\ \mathbf{0} & (\mathbf{R}_0^s(\theta^*))^{\mathrm{T}} \end{bmatrix}}_{\mathbf{L}(\mathbf{q},\theta^*)} \begin{bmatrix} \dot{\mathbf{y}}_t \\ \dot{\mathbf{y}}_r \end{bmatrix}, \tag{4.20}$$

with $\begin{bmatrix}\dot{\mathbf{y}}_t^{\mathrm{T}} & \dot{\mathbf{y}}_r^{\mathrm{T}}\end{bmatrix}^{\mathrm{T}}$ containing the end-effector Jacobian matrix that maps the joint velocities to the velocities of the task space,

$$\begin{bmatrix} \dot{\mathbf{y}}_t \\ \dot{\mathbf{y}}_r \end{bmatrix} = \mathbf{J}(\mathbf{q})\dot{\mathbf{q}}, \tag{4.21}$$

see [10]. By using the transformation $(\mathbf{R}_0^s(\theta^*))^{\mathrm{T}}$ in (4.20), see (4.18), the spool orientation is expressed in the reference frame of the current position on the path. Thus, two frames are used that are coupled to the path progress, the PT frame for the position and the reference frame for the spool orientation. Using both frames the position and orientation can be controlled relative to the path.

To obtain the mapping between the joint velocities $\dot{\mathbf{q}}$ and the velocities of the virtual output $\dot{\hat{\mathbf{y}}}$, the transformed Jacobian matrix

$$\hat{\mathbf{J}}(\mathbf{q}, \theta^*) = \mathbf{L}(\mathbf{q}, \theta^*)\mathbf{J}(\mathbf{q}) \tag{4.22}$$

Die approbierte gedruckte Originalversion dieser Diplomarbeit ist an der TU Wien Bibliothek verfügbar.
The approved original version of this thesis is available in print at TU Wien Bibliothek.

is introduced with the transformation according to

$$\dot{\hat{\mathbf{y}}} = \hat{\mathbf{J}}(\mathbf{q}, \theta^*)\dot{\mathbf{q}}. \tag{4.23}$$

Application of this new Jacobian results in a mapping of the configuration space $\mathbf{q} \in \mathbb{R}^7$ to the task space $\hat{\mathbf{y}} \in \mathbb{R}^6$, creating a one dimensional null space. The use of the transformation matrix $\mathbf{L}(\mathbf{q}, \theta^*)$ leads to a transformed Jacobian matrix $\hat{\mathbf{J}}(\mathbf{q}, \theta^*)$ of the form

$$\hat{\mathbf{J}}(\mathbf{q}, \theta^*) = \begin{bmatrix} \hat{\mathbf{J}}_t \\ \hat{\mathbf{J}}_r \end{bmatrix} = \begin{bmatrix} \hat{\mathbf{J}}_t \\ \hat{\mathbf{J}}_{r,e_x} \\ \hat{\mathbf{J}}_{r,e_y} \\ \hat{\mathbf{J}}_{r,e_z} \end{bmatrix}_{\mathbb{R}^{6\times 7}} . \tag{4.24}$$

The translational part in (4.24) is described by $\hat{\mathbf{J}}_t(\mathbf{q}, \theta^*)$ whereas $\hat{\mathbf{J}}_{r,e_{\{x,y,z\}}}(\mathbf{q}, \theta^*)$ denote the rotational motion relative to the coordinate axes of the reference frame. Due to the composition of this matrix the z-rotation of the spool can be isolated and transferred to the null space of the robot. Note that since the PT frame, defined by (4.9), and the reference frame transformation $(\mathbf{R}_0^s(\theta^*))^{\mathrm{T}}$ are used in $\mathbf{L}(\mathbf{q}, \theta^*)$, the geometry and orientation of the path is incorporated into the new virtual output.

4.3 Extended Null Space

As stated earlier, the KUKA *iiwa* is a redundant robot, which means it has more DOF than its task space ($\mathbf{q} \in \mathbb{R}^7$, $\mathbf{y} \in \mathbb{R}^6$). The remaining freedom is a motion in the null space. From the previous derivation, the null space is of dimension one but can be altered by the choice of an output if that is desired for the task, see [20].

Since the spool on the end-effector of the robot is rotationally symmetric, controlling the orientation around the z-axis of the spool is not necessary. By transferring this rotational DOF to the null space of the primary task, defined by ($\mathcal{O}1$)-($\mathcal{O}3$), this additional degree of freedom can be utilized to fulfill a further subtask. To isolate the z-rotation of the spool the transformed Jacobian matrix (4.24) is considered. This matrix describes the spool position relative to the current point on the path and the spool orientation in the reference frame. By removing the z-entry $\hat{\mathbf{J}}_{r,e_z}(\mathbf{q}, \theta^*)$ from

$$\hat{\mathbf{J}}(\mathbf{q}, \theta^*) = \begin{bmatrix} \hat{\mathbf{J}}_t \\ \hat{\mathbf{J}}_{r,e_x} \\ \hat{\mathbf{J}}_{r,e_y} \\ \hat{\mathbf{J}}_{r,e_z} \end{bmatrix}_{\mathbb{R}^{6\times 7}} \tag{4.25}$$

and $\dot{\hat{\mathbf{J}}}(\mathbf{q}, \theta^*)$ the z-rotation is neglected and hence remains uncontrolled. The reduced end-effector Jacobian matrix results in

$$\tilde{\mathbf{J}}(\mathbf{q}, \theta^*) = \begin{bmatrix} \hat{\mathbf{J}}_t \\ \hat{\mathbf{J}}_{r,e_x} \\ \hat{\mathbf{J}}_{r,e_y} \end{bmatrix}_{\mathbb{R}^{5\times 7}} , \tag{4.26}$$

Die approbierte gedruckte Originalversion dieser Diplomarbeit ist an der TU Wien Bibliothek verfügbar.
The approved original version of this thesis is available in print at TU Wien Bibliothek.
TU Bibliothek Your knowledge hub WIEN

which leads to

$$\dot{\tilde{\mathbf{y}}} = \tilde{\mathbf{J}}(\mathbf{q}, \theta^*)\dot{\mathbf{q}} = \begin{bmatrix} \hat{\mathbf{J}}_t \\ \hat{\mathbf{J}}_{r,e_x} \\ \hat{\mathbf{J}}_{r,e_y} \end{bmatrix} \dot{\mathbf{q}}. \tag{4.27}$$

This reduction of the rows in the Jacobian matrices results in a reduced task space for the robot.

Using (4.26) a subtask can be formulated by applying a null space projection. The null space projection matrix is defined in [20] by

$$\mathbf{N}_J(\mathbf{q}, \theta^*) = \Big(\mathbf{I} - \tilde{\mathbf{J}}^{\mathrm{T}}(\mathbf{q}, \theta^*)\tilde{\mathbf{J}}^{\mathbf{W}}(\mathbf{q}, \theta^*)\Big), \tag{4.28}$$

where $\mathbf{I}$ denotes the identity matrix and $\{\}^{\mathbf{W}}$ the inverse by applying a weighting matrix $\mathbf{W} \in \mathbb{R}^{n \times n}$ according to

$$\mathbf{A}^{\mathbf{W}} = \mathbf{W}^{-1}\mathbf{A}^{\mathrm{T}}\Big(\mathbf{A}\mathbf{W}^{-1}\mathbf{A}^{\mathrm{T}}\Big)^{-1}. \tag{4.29}$$

As outlined in [20], the use of the mass matrix of the current configuration as a weighting matrix, $\mathbf{W}(\mathbf{q}) = \mathbf{M}(\mathbf{q})$, results in a so called dynamically consistent projector. This describes that a subtask does not generate interfering forces or accelerations in the task space of higher priority tasks. Hence by choosing the right projector the tasks are decoupled.

The null space projector (4.28) is to be used in the following to implement a null space controller.

4.4 Feedback Linearization

In this section, a feedback transformation is introduced, establishing a linear relation between the input and the output of the system, see [10, 11].

Using the second time derivative of the reduced virtual output $\tilde{\mathbf{y}}$,

$$\ddot{\tilde{\mathbf{y}}} = \dot{\tilde{\mathbf{J}}}(\mathbf{q}, \theta^*)\dot{\mathbf{q}} + \tilde{\mathbf{J}}(\mathbf{q}, \theta^*)\ddot{\mathbf{q}} \tag{4.30}$$

and recalling the dynamic equations of the system,

$$\tilde{\mathbf{M}}(\mathbf{q})\ddot{\mathbf{q}} + \mathbf{n}(\mathbf{q}, \dot{\mathbf{q}}) = \boldsymbol{\tau} + \boldsymbol{\tau}_{ext}, \tag{4.31}$$

with

$$\mathbf{n}(\mathbf{q}, \dot{\mathbf{q}}) = \mathbf{C}(\mathbf{q}, \dot{\mathbf{q}})\dot{\mathbf{q}} + \mathbf{g}(\mathbf{q}), \tag{4.32}$$

a feedback transformation can be applied. Rearranging (4.31) for $\ddot{\mathbf{q}}$ and inserting into (4.30) yields,

$$\ddot{\tilde{\mathbf{y}}} = \dot{\tilde{\mathbf{J}}}(\mathbf{q}, \theta^*)\dot{\mathbf{q}} + \tilde{\mathbf{J}}(\mathbf{q}, \theta^*)\Big[\tilde{\mathbf{M}}(\mathbf{q})^{-1}(\boldsymbol{\tau} + \boldsymbol{\tau}_{ext} - \mathbf{n}(\mathbf{q}, \dot{\mathbf{q}}))\Big]. \tag{4.33}$$

Using the state feedback

$$\boldsymbol{\tau} = \mathbf{n}(\mathbf{q}, \dot{\mathbf{q}}) - \boldsymbol{\tau}_{ext} + \tilde{\mathbf{M}}(\mathbf{q})\,\tilde{\mathbf{J}}^{\dagger}(\mathbf{q}, \theta^*)\Big(\mathbf{v} - \dot{\tilde{\mathbf{J}}}(\mathbf{q}, \theta^*)\dot{\mathbf{q}}\Big) + \boldsymbol{\tau}_N \tag{4.34}$$

Die approbierte gedruckte Originalversion dieser Diplomarbeit ist an der TU Wien Bibliothek verfügbar.
The approved original version of this thesis is available in print at TU Wien Bibliothek.
TU Bibliothek Your knowledge hub WIEN

in (4.33), with the pseudoinverse

$$\tilde{\mathbf{J}}^{\dagger}(\mathbf{q},\theta^*) = \tilde{\mathbf{J}}^{\mathrm{T}}(\mathbf{q},\theta^*)\Big(\tilde{\mathbf{J}}(\mathbf{q},\theta^*)\,\tilde{\mathbf{J}}^{\mathrm{T}}(\mathbf{q},\theta^*)\Big)^{-1}, \tag{4.35}$$

yields $\ddot{\tilde{\mathbf{y}}} = \mathbf{v}$, with the new control input $\mathbf{v}$. The expression $\boldsymbol{\tau}_N$ in (4.34) denotes the generalized torques resulting from the null space controller, which is to be defined in the following. The new control input $\mathbf{v}$ contains entries for every subsystem, i. e.,

$$\mathbf{v} = \begin{bmatrix} \mathbf{v}_t \\ \mathbf{v}_r \end{bmatrix} = \begin{bmatrix} v_{t,1} \\ v_{t,2} \\ v_{t,3} \\ v_{r,e_x} \\ v_{r,e_y} \end{bmatrix}. \tag{4.36}$$

With this new control input $\mathbf{v}$ the respective subsystems can be controlled separately. As in [10] the control input $\mathbf{v}$ is used to meet the desired control objectives ($\mathcal{O}1$) and ($\mathcal{O}2$) by setting $v_{t,2} = 0$ and $v_{t,3} = 0$ and using a linear controller to asymptotically stabilize the system. Since the control input $v_{t,1}$ controls the tangential motion on the path also ($\mathcal{O}3$) is fulfilled.

4.5 Control

For the following considerations, the error vector $\tilde{\mathbf{e}}$ is split into a translational and rotational part, i. e., $\tilde{\mathbf{e}}_t$ and $\tilde{\mathbf{e}}_r$, respectively. By using a compliance control law (PD controller) a desired behavior can be imposed on the subsystems of the robot. The new control input for the translational subsystem $\mathbf{v}_t$ is chosen as

$$\mathbf{v}_t = \ddot{\tilde{\mathbf{y}}}_t^d - \mathbf{K}_{1,t}\,\dot{\tilde{\mathbf{e}}}_t - \mathbf{K}_{0,t}\,\tilde{\mathbf{e}}_t, \tag{4.37}$$

with the translational error vector

$$\tilde{\mathbf{e}}_t = \Big(\tilde{\mathbf{y}}_t - \tilde{\mathbf{y}}_t^d\Big) = \begin{bmatrix} \eta - \eta^d \\ \xi_1 - \xi_1^d \\ \xi_2 - \xi_2^d \end{bmatrix} \tag{4.38}$$

and its derivative $\dot{\tilde{\mathbf{e}}}_t = (\dot{\tilde{\mathbf{y}}}_t - \dot{\tilde{\mathbf{y}}}_t^d)$. The values for the desired tangential and transversal direction are denoted by η^d and $\xi_{\{1,2\}}^d$, respectively. The consequent error dynamic

$$\ddot{\tilde{\mathbf{e}}}_t + \mathbf{K}_{1,t}\dot{\tilde{\mathbf{e}}}_t + \mathbf{K}_{0,t}\tilde{\mathbf{e}}_t = \mathbf{0} \tag{4.39}$$

is exponentially stable if the matrices $\mathbf{K}_{1,t}$ and $\mathbf{K}_{0,t}$ are of diagonal form with entries $k_{1,t_i} > 0$ and $k_{0,t_i} > 0$ for $i = 1, \ldots, 3$. The used values for these matrices are listed in Appendix A.1.5.

The orientation error $\tilde{\mathbf{e}}_r$ is calculated from the error quaternion $\mathbf{e}_{\mathcal{Q}}$ describing the difference between the current and the desired spool orientation. With $\mathcal{Q}^d$ and $\mathcal{Q}_e$

Die approbierte gedruckte Originalversion dieser Diplomarbeit ist an der TU Wien Bibliothek verfügbar.
The approved original version of this thesis is available in print at TU Wien Bibliothek.
TU Bibliothek Your knowledge hub WIEN

representing the quaternions of the desired and current spool orientation, respectively, the quaternion product yields

$$\mathbf{e}_{\mathcal{Q}} = \{\mu \quad \boldsymbol{\epsilon}\} = \mathcal{Q}^d \otimes \mathcal{Q}_e^{-1}, \tag{4.40}$$

with the scalar part μ and the vector part $\boldsymbol{\epsilon}$. For the resulting quaternion, $\mathbf{e}_{\mathcal{Q}} = \{\mu \quad \mathbf{0}\}$ holds if and only if the two orientations are aligned, see [14] and [21]. To correspond with the reduced dimension of the task space, the last entry of the vector part of the error quaternion is omitted

$$\tilde{\mathbf{e}}_r = \begin{bmatrix} \epsilon_1 \\ \epsilon_2 \end{bmatrix}. \tag{4.41}$$

The control input for the rotational subsystem $\mathbf{v}_r$ is formed according to

$$\mathbf{v}_r = \dot{\boldsymbol{\omega}}^d - \mathbf{K}_{1,r}\left(\boldsymbol{\omega} - \boldsymbol{\omega}^d\right) - \mathbf{K}_{0,r}\tilde{\mathbf{e}}_r, \tag{4.42}$$

using the angular velocity vector of the spool $\boldsymbol{\omega}$ and its desired value $\boldsymbol{\omega}^d$. The corresponding error system results in

$$\left(\dot{\boldsymbol{\omega}} - \dot{\boldsymbol{\omega}}^d\right) + \mathbf{K}_{1,r}\left(\boldsymbol{\omega} - \boldsymbol{\omega}^d\right) + \mathbf{K}_{0,r}\tilde{\mathbf{e}}_r = \mathbf{0}. \tag{4.43}$$

The desired angular velocity vector $\boldsymbol{\omega}^d$ is formed by means of the reference frame $\mathbf{R}_0^s(\theta^*)$ and its derivative as in (2.7),

$$\mathbf{S}(\boldsymbol{\omega}_{0,0}^s) = \dot{\mathbf{R}}_0^s(\theta^*)\dot{\theta}^*(\mathbf{R}_0^s(\theta^*))^{\mathrm{T}}. \tag{4.44}$$

The resulting vector $\boldsymbol{\omega}_{0,0}^s$ describes the angular velocity of the spool frame with respect to the base CS, expressed in the base CS. To isolate the z-rotation to correspond with the reduced task space, the angular velocity vector is transformed to the reference frame according to

$$\boldsymbol{\omega}_{0,s}^s = (\mathbf{R}_0^s(\theta^*))^{\mathrm{T}}\,\boldsymbol{\omega}_{0,0}^s. \tag{4.45}$$

In the desired angular velocity vector the z-axis is omitted which yields

$$\boldsymbol{\omega}^d = \begin{bmatrix} \omega_{0,s_x}^s \\ \omega_{0,s_y}^s \end{bmatrix}. \tag{4.46}$$

The desired angular acceleration vector $\dot{\boldsymbol{\omega}}^d$ is the time derivative of (4.46). A proof of stability of an error system with the use of the whole vector part of the quaternion $\boldsymbol{\epsilon}$ and the whole angular velocity vector $\boldsymbol{\omega}_{0,s}^s$ is given in [14] and [21]. However, since the error system (4.43) contains only two entries per vector, this approach is not directly applicable.

The chosen objective of the subtask, which is controlled by the null space controller, is to keep the robot axes near their neutral position $\mathbf{q}_0 = \mathbf{0}$ to avoid the axis limits of the robot. Using the suggested projector from (4.28), a PD controller is formulated according to

$$\boldsymbol{\tau}_{\mathrm{N}} = \mathbf{N}_J(\mathbf{q}, \theta^*)(-\mathbf{K}_{\mathrm{N}1}\dot{\mathbf{q}} - \mathbf{K}_{\mathrm{N}0}(\mathbf{q} - \mathbf{q}_0)) \tag{4.47}$$

to stabilize the desired position $\mathbf{q}_0$. The positive definite diagonal matrices $\mathbf{K}_{\mathrm{N}1}$ and $\mathbf{K}_{\mathrm{N}0}$ denote the derivative and proportional gain matrices, respectively. The expression

Die approbierte gedruckte Originalversion dieser Diplomarbeit ist an der TU Wien Bibliothek verfügbar.
The approved original version of this thesis is available in print at TU Wien Bibliothek.
TU Bibliothek Your knowledge hub WIEN

$\boldsymbol{\tau}_\mathrm{N}$ refers to the generalized torques from the null space controller, which is used in the feedback linearization (4.34). With this control concept, the robot is able to follow the path and control the x- and y-orientation of the spool. The orientation around the spool axis, (z-axis) however, is determined by (4.47) and reduces the risk of hitting an axis limit. The values for the used control variables are listed in Appendix A.1.5.

Note that the original task space contained three DOF for position and three DOF for orientation whereas the new task space omits the rotation around the z-axis of the spool, hence five DOF remain. A schematic drawing of the control structure is shown in Figure 4.2.

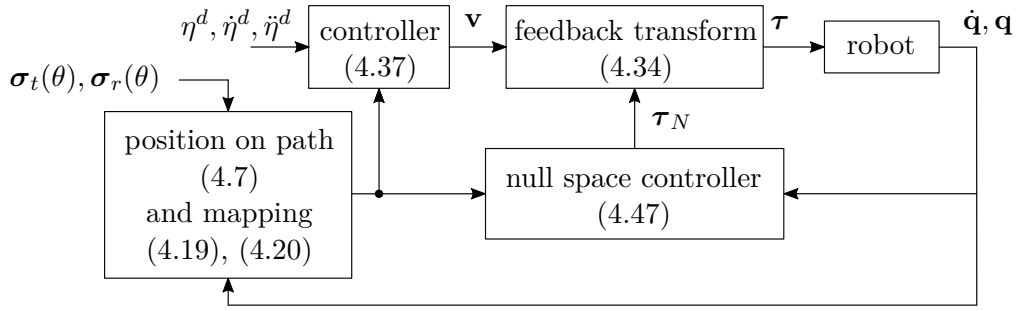

Figure 4.2: Block diagram of the control structure.

4.6 Path Progression

In this section, the discrete-time calculation of (4.7) and (4.10) is described.

The motion along the path can be controlled using the expressions η^d, ξ_1^d and ξ_2^d. The expressions ξ_1^d, ξ_2^d and their derivatives are set to zero to control the transversal motion along the path to be zero. The progress of η^d is controlled using a set-point filter, similar to [12]. The output of the filter is a trajectory for the desired values η^d, $\dot{\eta}^d$ and $\ddot{\eta}^d$ where the first derivative and thus the velocity to a desired maximal value v_{max} is limited.

For the implementation of the optimization problem in a digital computer, (4.7) is solved numerically according to

$$\theta_{k,i} = \theta_{k,i-1} - \frac{J'(\theta_{k,i-1})}{J''(\theta_{k,i-1})}, \tag{4.48}$$

using the Newton method as shown in [10]. The cost function is given by $J(\theta_{k,i-1}) = \|\mathbf{y}_{t,k} - \boldsymbol{\sigma}_t(\theta_{k,i-1})\|_2^2$. The optimal solution $\theta_k^* = \theta_{k,i}$ is used in the numeric integration of (4.10) to get the arc length

$$\eta_k = \eta_{k-1} + (\theta_k^* - \theta_{k-1}^*)\|\boldsymbol{\sigma}_t'(\theta_k^*)\|_2. \tag{4.49}$$

Die approbierte gedruckte Originalversion dieser Diplomarbeit ist an der TU Wien Bibliothek verfügbar.
The approved original version of this thesis is available in print at TU Wien Bibliothek.
TU Bibliothek Your knowledge hub WIEN

5 Implementation and Results

After the description of the model, tool and the PFC strategy, this chapter is concerned with the details of the implementation and the experimental results.

In the first section, the teach-in procedure is discussed. The hardware setup is described in addition to the post-processing steps of the measurement. These are performed to construct a smooth curve and to synchronize the path with the torque information from the teach-in tool.

In the following sections, the setup for the reenactment is described. Furthermore, the simulation and experimental results are presented.

5.1 Experimental Setup – Teach-In Phase

The task demonstration is recorded using the software MOTIVE from OPTITRACK with four cameras placed around the area of interest. After calibration, the system tracks a previously defined body consisting of infrared markers, in this case the marker body described in Chapter 3. Note that the robot has no additional information regarding obstacles, e. g., rods, within its workspace. The necessary information is provided by the operator during teach-in and by setting the relative distances of the OPTITRACK and robot CS.

In Figure 5.1, the block diagram for the task demonstration is depicted. During teach-in the information is gathered on a single computer where MOTIVE and TWINCAT are installed. The switch and the bus coupler are connected to the network interface cards (NIC) of the computer.

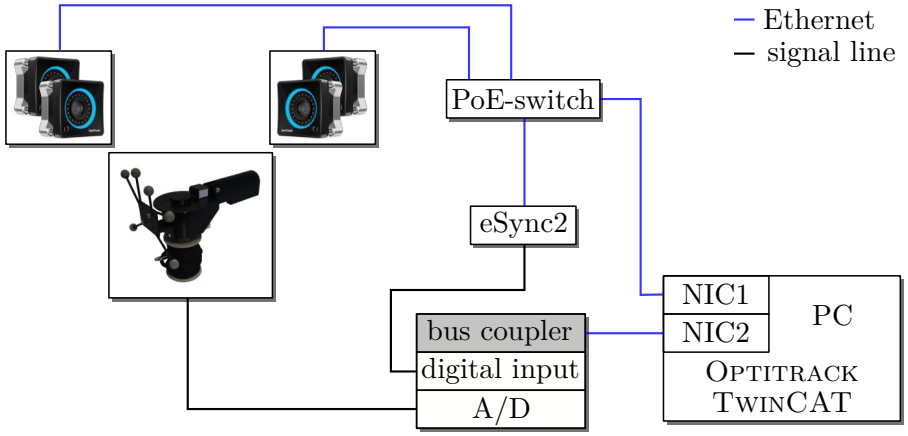

Figure 5.1: Block diagram of the setup for the teach-in of the task.

Die approbierte gedruckte Originalversion dieser Diplomarbeit ist an der TU Wien Bibliothek verfügbar.
The approved original version of this thesis is available in print at TU Wien Bibliothek.

An eSync2 box, also from OPTITRACK, is utilized for the synchronization of the tracking data from the cameras with the torque data measured by the rotary torque sensor. The internal clock signal of the OPTITRACK system in addition to a recording-on signal is output by eSync2 and measured by a digital I/O-terminal of a BECKHOFF PLC system. The force and clock signals are read by the I/O-terminals and gathered in TWINCAT. OPTITRACK was set to use an internal clock frequency of 100 Hz, the internal clock of the TWINCAT system was set to 1 kHz. The utilized BECKHOFF I/O-terminals are listed below.

- EK1814: ETHERCAT bus coupler with integrated digital I/Os
- EL3101: analog input terminal, Input: −10 V to +10 V, 16 bit for the measurement of the torque signal
- EL9505: power supply converter terminal, Input: 24 V, Output: 5 V
- EL1124: 4-channel digital input terminal, Input: 5 V for measurement of the signals from eSync2

When performing the teach-in both TWINCAT and MOTIVE are in recording mode. The measured data is stored for the following post-processing of the pose and force information. Figure 5.2 shows the setup with the rods placed for the winding of a rope.

(a) Before the start of the demonstration. (b) After the demonstration is finished.

Figure 5.2: Setup for the teach-in process. The tool is moved around the rods to unwind the rope and apply the desired tension, as visualized by the bent rod in (b).

In Figure 5.2(a), the tool is placed in the demonstration area. During teach-in the rope is wound around the rods while applying a desired force by using the breaking mechanism of the teach-in tool. This is visualized by the bent rod in Figure 5.2(b), which is due to the applied rope tension. The gathered measurements are post-processed which is described in the next section.

Path Post-Processing

After the teach-in is completed, the acquired data needs to be processed to obtain valid path and force information for the robot to perform the desired task. Small movements of the operator during teach-in in addition to measurement noise result in a rough shape

Die approbierte gedruckte Originalversion dieser Diplomarbeit ist an der TU Wien Bibliothek verfügbar.
The approved original version of this thesis is available in print at TU Wien Bibliothek.
TU Bibliothek Your knowledge hub WIEN

of the path. This requires additional smoothing of the curve to meet the criteria for an admissible path defined in Section 4.1. Furthermore, regions of little or no motion need to be handled, e. g., at the beginning or end of the teach-in phase when the teach-in tool is inside the demonstration area but not moved by the operator. Additionally, the torque signal is smoothed and synchronized with the OPTITRACK measurement. The flowchart in Figure 5.3 shows the performed steps during post-processing of the measurement.

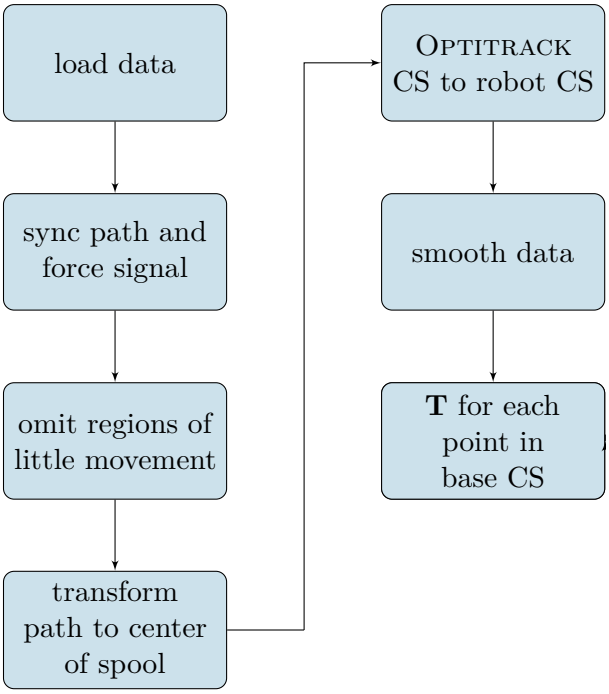

Figure 5.3: Procedure of post-processing.

Initially, the digital signal of the torque sensor is converted to an equivalent torque by using the conversion factor,

$$\frac{10\,\mathrm{V}}{2^{15}\mathrm{Bit}}\,\frac{2\,\mathrm{N\,m}}{5\,\mathrm{V}} = 1.22\cdot 10^{-4}\frac{\mathrm{N\,m}}{\mathrm{Bit}}. \tag{5.1}$$

Next, the synchronization of the OPTITRACK position and the TWINCAT force signals is done. Since the torque signal is sampled at a higher rate (1 kHz) compared to the position signal (100 Hz) it needs to be downsampled. For each sampling period, the mean value of the torque is calculated. The result can be seen in Figure 5.4. The first image shows the measured signal, the second image shows the signal with reduced points and shifted to $t = 0\,\mathrm{s}$.

To omit parts of the measurement without active motion, regions of little or no movement are identified and erased. The Euclidean distance of the points in 3D provides a measure to detect these regions. Measurement points of 100 and more samples with a distance smaller than $d_{min} = 1\,\mathrm{cm}$ are omitted from further processing. These points are then replaced by their mean value.

Die approbierte gedruckte Originalversion dieser Diplomarbeit ist an der TU Wien Bibliothek verfügbar.
The approved original version of this thesis is available in print at TU Wien Bibliothek.
TU Bibliothek Your knowledge hub WIEN

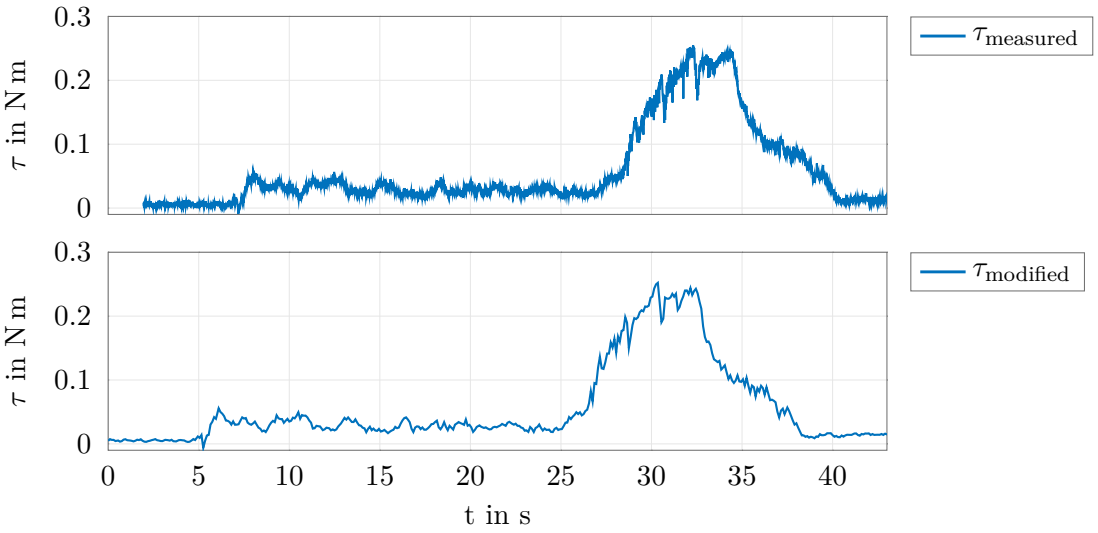

Figure 5.4: Processing of the measured torque signal.

Next, the acquired position data is transformed to the center position of the spool. The distances are obtained from the CAD data of the teach-in tool as described in Section 3.3 and shown in Figure 3.4. The result is depicted in Figure 5.5. Note that the coordinates are plotted in the CS defined by the tracking system.

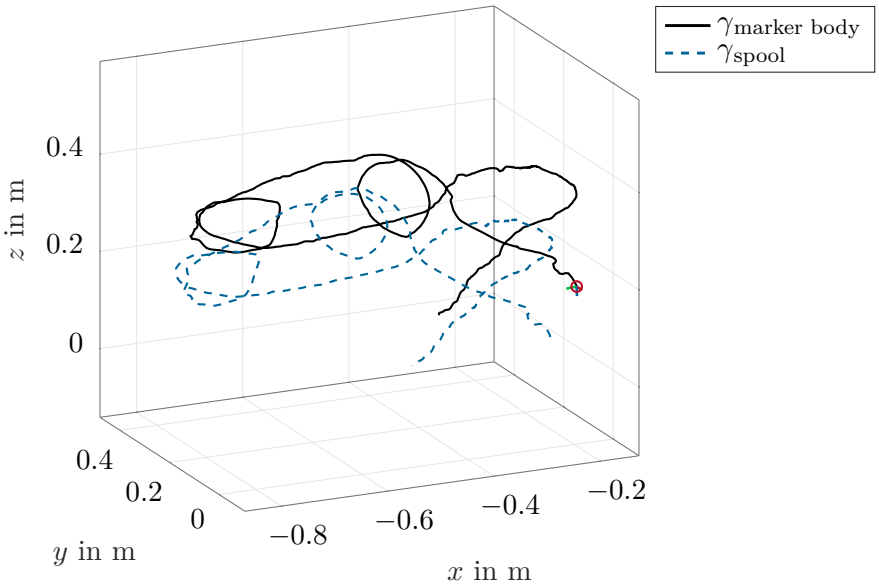

Figure 5.5: Path of spool center relative to the measured path of the OPTITRACK marker.

After transforming the curves to the base CS of the robot, the data is filtered using a Savitzky-Golay filter. The frame length of the filter m_f was calculated depending on the

Die approbierte gedruckte Originalversion dieser Diplomarbeit ist an der TU Wien Bibliothek verfügbar.
The approved original version of this thesis is available in print at TU Wien Bibliothek.

number of obtained data points n_M. Filter lengths ranging from $\frac{n_M}{20}$ to $\frac{n_M}{30}$ showed to smooth the path sufficiently while still preserving the shape. In this case, a filter length of $m_f = 119$ for $n_M = 3328$ measured points was used.

The remaining points are downsampled by a factor 15 to reduce the number of data points. This proved to be useful since it results in smoother first and second derivatives of the path. All remaining points and related orientations are assembled in a respective homogeneous transformation matrix $\mathbf{T}$. The resulting path is depicted in Figure 5.6 with the reference frames indicated along the path.

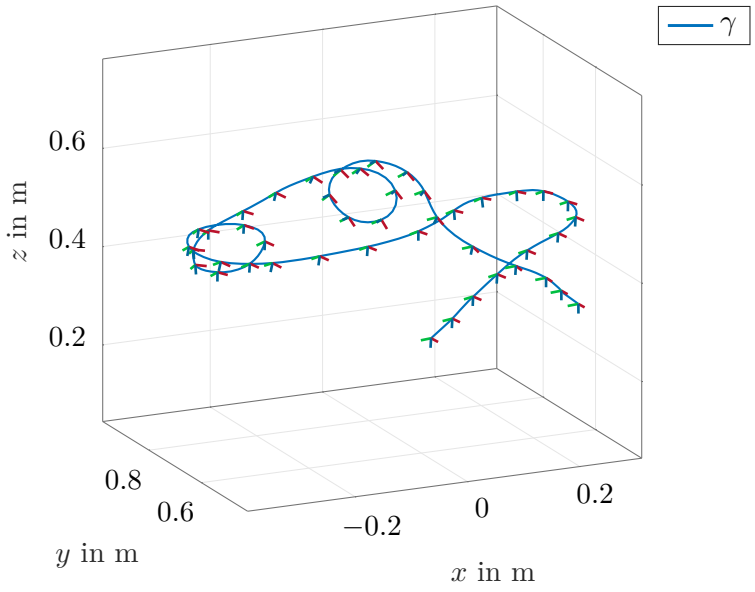

Figure 5.6: Smoothed curve after post-processing with indicated reference frames to denote for the change of orientation along the path.

The smoothing of the torque data is done likewise with a Savitzky-Golay filter of length $1.4\,m_f$. The resulting parametrized spline curve is depicted in Figure 5.7. The spline is normalized to $\theta \in [0, 1]$ corresponding to the path, with θ being the path parameter, see Chapter 4.

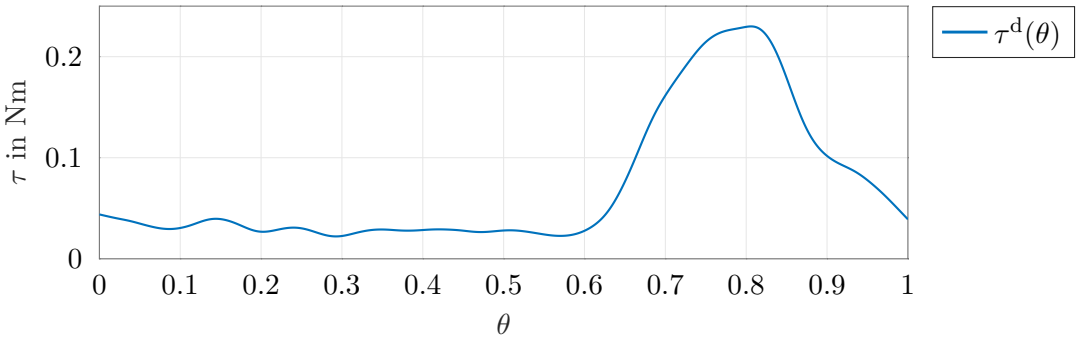

Figure 5.7: Smoothed spline curve representing the recorded torque signal.

Die approbierte gedruckte Originalversion dieser Diplomarbeit ist an der TU Wien Bibliothek verfügbar.
The approved original version of this thesis is available in print at TU Wien Bibliothek.

From the obtained homogeneous transformations $\mathbf{T}$ a basis spline (B-spline) is constructed which is then provided to the PFC. To obtain a unit quaternion curve, representing the change of orientation along the path, an implementation of the findings of [22, 23] is utilized. The advantage of the proposed method is that it is able to construct a quaternion curve that preserves C^k continuity.

5.2 Experimental Setup – Reenactment Phase

The verification of the successful teach-in and reenactment is demonstrated using a KUKA LBR iiwa 14 R820 robot. A rope-winding task is demonstrated using the designed tool to wind a rope around arbitrarily placed rods, see Figure 5.2. The demonstrated task is then reproduced by the robot during the reenactment phase.

For the experiment, the KUKA *iiwa* is controlled via a BECKHOFF TWINCAT system which executes a compiled MATLAB/Simulink model containing the control logic. Using the BECKHOFF standard ETHERCAT, all the hardware is connected to a central computer establishing real-time communication between the components. Two network interface cards (NIC) are utilized. One is solely used for the communication with the robot, the second one is connected to the motor controller and the flange of the robot. In TWINCAT the sensor data of the robot, e. g. position and torque of the joints, are measured. The desired joint torque is computed in the MATLAB/Simulink model and output by TWINCAT to control the robot motion. The experimental setup is depicted in Figure 5.8.

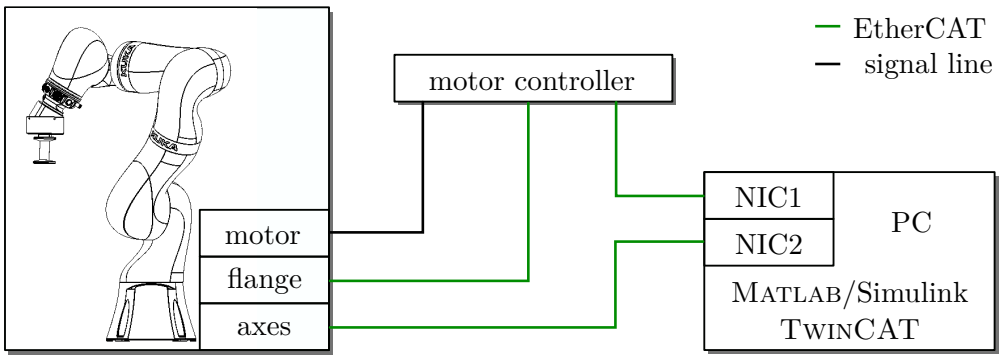

Figure 5.8: Block diagram of the experimental setup.

Since the sampling time of $T_s = 125\,\mu s$ was too fast to finish the computations performed by the path following controller (PFC) within one cycle, the MATLAB/Simulink model was split into a fast and slow model. Both models are executed on separate CPU (Central Processing Unit) cores on the computer. The fast model, implementing the singular perturbation controller that accounts for the joint elasticity, runs with a sampling time of $T_{s_{fast}} = 125\,\mu s$. The slow subsystem contains the control logic for the PFC and is set to $T_{s_{slow}} = 500\,\mu s$. This ensures that the computationally expensive PFC computations are finished within one sampling interval, ensuring real-time communication. Note that the use of the fast sampling time of $T_{s_{fast}} = 125\,\mu s$ is necessary to control the fast joint dynamics. Hence the system was split into a fast and slow subsystem instead of increasing

Die approbierte gedruckte Originalversion dieser Diplomarbeit ist an der TU Wien Bibliothek verfügbar.
The approved original version of this thesis is available in print at TU Wien Bibliothek.
TU Bibliothek Your knowledge hub WIEN

the sampling time of the overall system.

As already described in Chapter 2, the spool and the motor are mounted on the flange of the robot, in a tilted position, see Figure 5.9. This enables the robot to take kinematically more favorable configurations for different placements of the rods.

Figure 5.9: Spool and motor and the robot tilted around the y-axis, see also Figure 2.2.

An example setup for the rods is depicted in Figure 5.2. The tilted spool not only extends the range and hence the workspace of the robot it also keeps axis q_6 ("wrist") further away from its maximum joint angle. Since axis q_6 has a range of $\theta_{6_{max}} = \pm 120°$, see Appendix A.1.1, moving near a stretched configuration with the spool pointing downwards approaches this limit. This is especially the case for the current application when winding around vertical rods. Hence enabling a kinematically more beneficial pose means that the robot is less likely to violate an axis limit.

For better visualization of the applied torque during the demonstration and reenactment phase, one of the rods has a flexible mount. Figure 5.10 shows the wound rope during task demonstration with one of the rods in a bent position due to the applied tension during teach-in.

The measured spool torque, which is applied to tension the rope, is available as a parametrized spline as described in Section 5.1. The progress of the path and torque signal is synchronized by θ. The desired rated motor torque τ_r^d is calculated in MATLAB/Simulink according to

$$\tau_r^d = \frac{\tau^d(\theta^*)}{\tau_{m_N}} \tag{5.2}$$

and provided to the motor controller hardware which uses a PI controller to set the torque. The expression $\tau^d(\theta^*)$ denotes the desired torque as depicted in Figure 5.7. The nominal motor torque results from the motor parameters in $\tau_{m_N} = 518.8\,\text{mN m}$. The motor and controller parameters for the motor controller are listed in Appendix A.1.2.

Die approbierte gedruckte Originalversion dieser Diplomarbeit ist an der TU Wien Bibliothek verfügbar.
The approved original version of this thesis is available in print at TU Wien Bibliothek.
TU Bibliothek Your knowledge hub WIEN

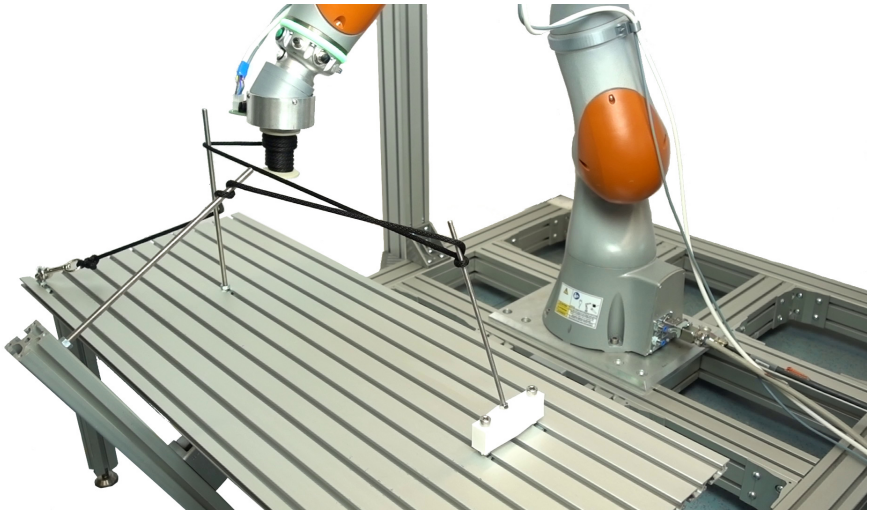

Figure 5.10: Robot during the reenactment phase of the demonstrated task. The rope is wound around the desired rods with the desired rope tension applied.

5.3 Simulation Results

In this section, the simulation results are presented and discussed. The simulation shows the motion and torques for the demonstrated path. Note that only the path following behavior is simulated. No external forces acting on the end-effector of the robot are considered. Apart from that the simulation uses the same MATLAB/Simulink model as for the experiment. The controller parameters used in this section are listed in Appendix A.1.5. The simulation starts at $t = 10$s since the relevant path following segment begins at this time.

The control errors are displayed in Figure 5.11. The first plot depicts the errors in tangential and transversal direction from the path. Note that despite the error signal changes considerably during the process its magnitude is in the range of $1 \cdot 10^{-4}$ m.

The second plot in Figure 5.11 shows the orientation error for the spool. Since the rotation around the z-axis of the spool is transferred to the null space, as described in Section 4.3, only the rotation around the x-axis and y-axis are depicted. Note that these two error signals are two quaternion entries, hence no unit is given on the y-axis. The angle Δ_r, which describes the difference between the z-axis rotation in rad during teach-in and reenactment, is shown in the third plot.

The distance from the desired path according to the Euclidean distance $d = \left\|\mathbf{x} - \mathbf{x}^d\right\|$ is depicted in the last plot of Figure 5.11. As can be seen the controller performs well in the simulation with small deviations from the desired path.

Figure 5.12 shows the joint angles over time. In addition to the joint angles the joint limits are marked according to the values listed in Appendix A.1.1. In the simulation, the joint q_4 is of particular interest.The setup for the reenactment in this scenario is placed next to the robot at about 25 cm from the robot base in z-direction, see Figure 5.10. This means that the axis q_4 ("elbow") performs a large part of the motion while traversing

Die approbierte gedruckte Originalversion dieser Diplomarbeit ist an der TU Wien Bibliothek verfügbar.
The approved original version of this thesis is available in print at TU Wien Bibliothek.
TU Bibliothek Your knowledge hub WIEN

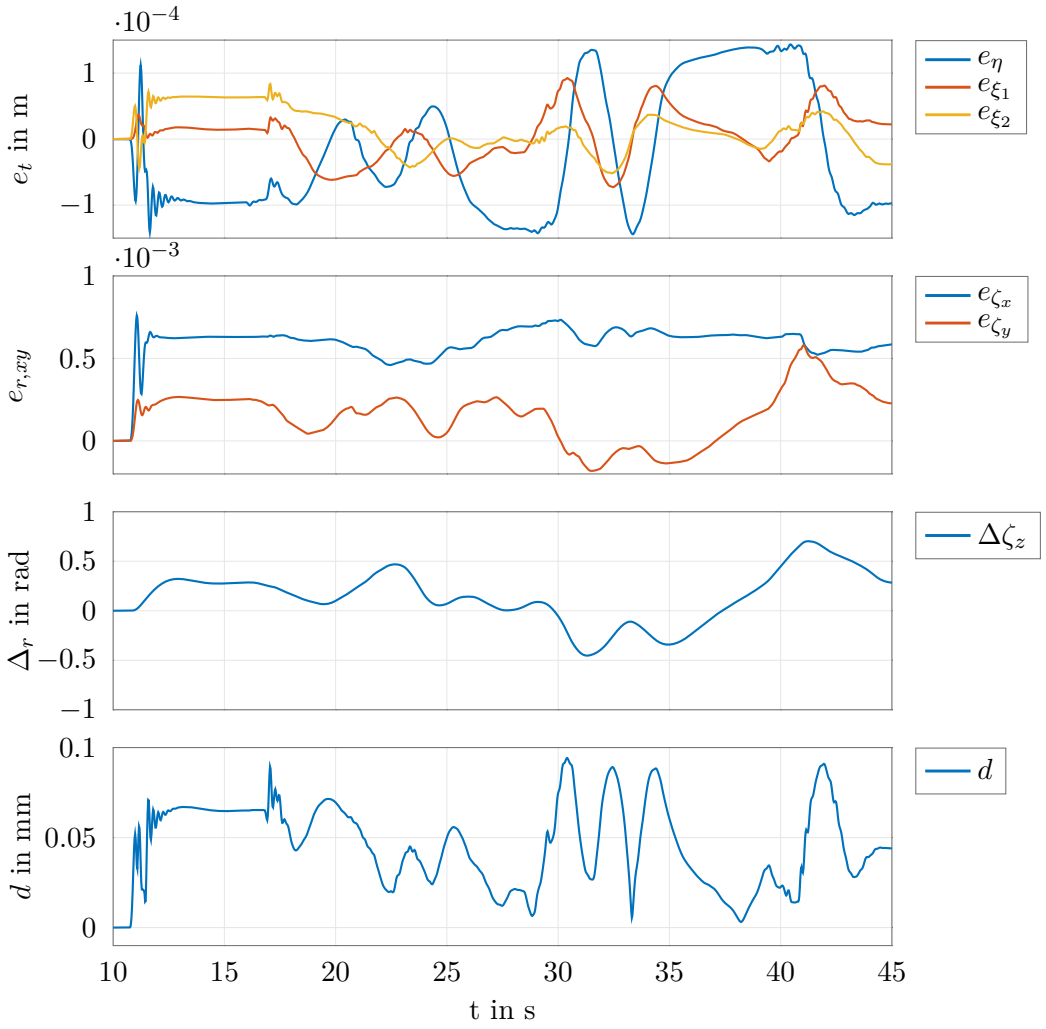

Figure 5.11: Control errors and distance from the path in the simulation.

through the path, which leads to axis q_4 approaching its joint limit if the path comes too close to the robot. Hence the simulation shows clearly if the path is applicable.

The torques, resulting from the simulation, are shown in Figure 5.13 for each respective axis. No significant torque peaks can be seen, which means that the path is traversed smoothly.

Die approbierte gedruckte Originalversion dieser Diplomarbeit ist an der TU Wien Bibliothek verfügbar.
The approved original version of this thesis is available in print at TU Wien Bibliothek.
TU Bibliothek Your knowledge hub WIEN

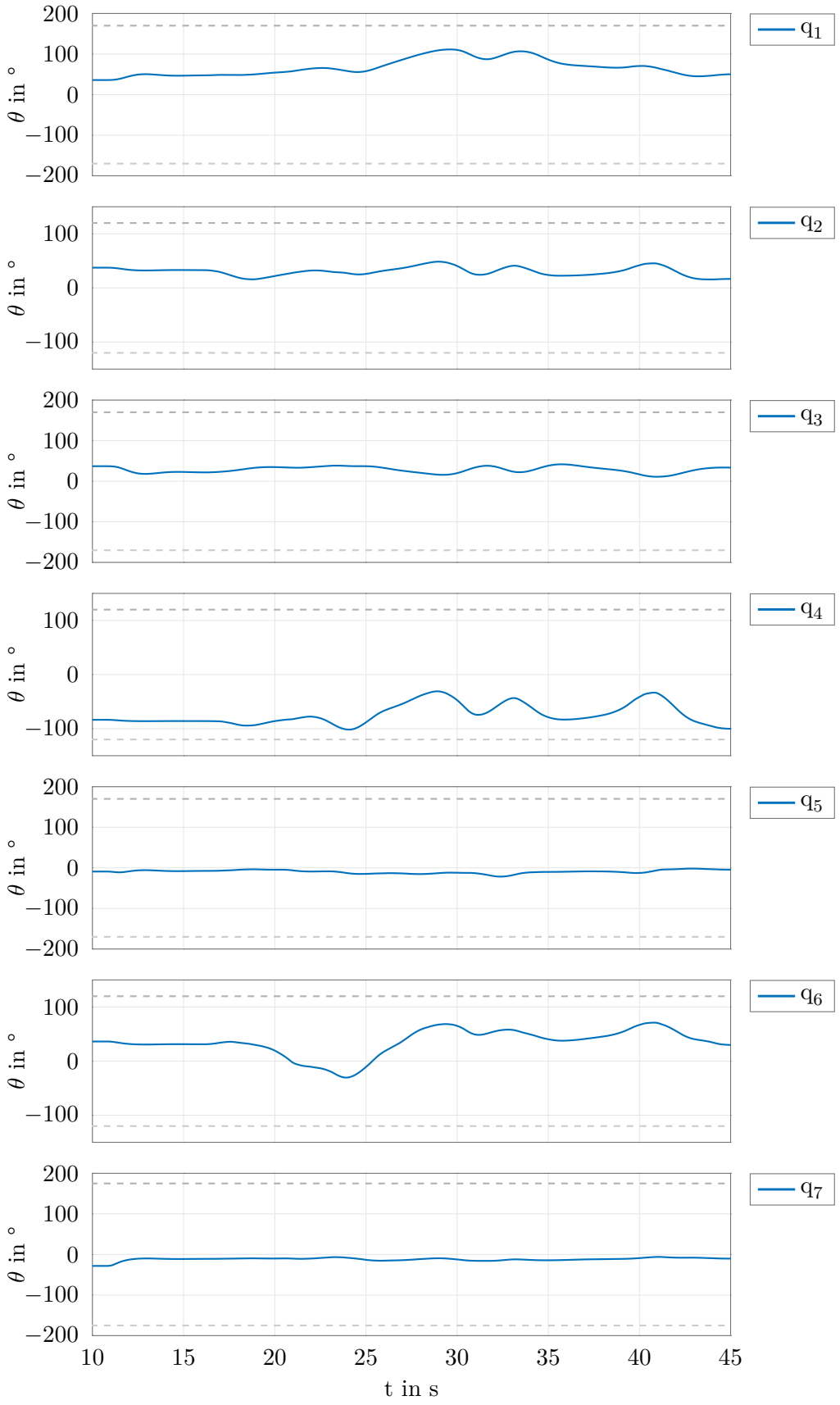

Figure 5.12: Joint angles in the simulation with the joint limits (dashed lines).

Die approbierte gedruckte Originalversion dieser Diplomarbeit ist an der TU Wien Bibliothek verfügbar.
The approved original version of this thesis is available in print at TU Wien Bibliothek.

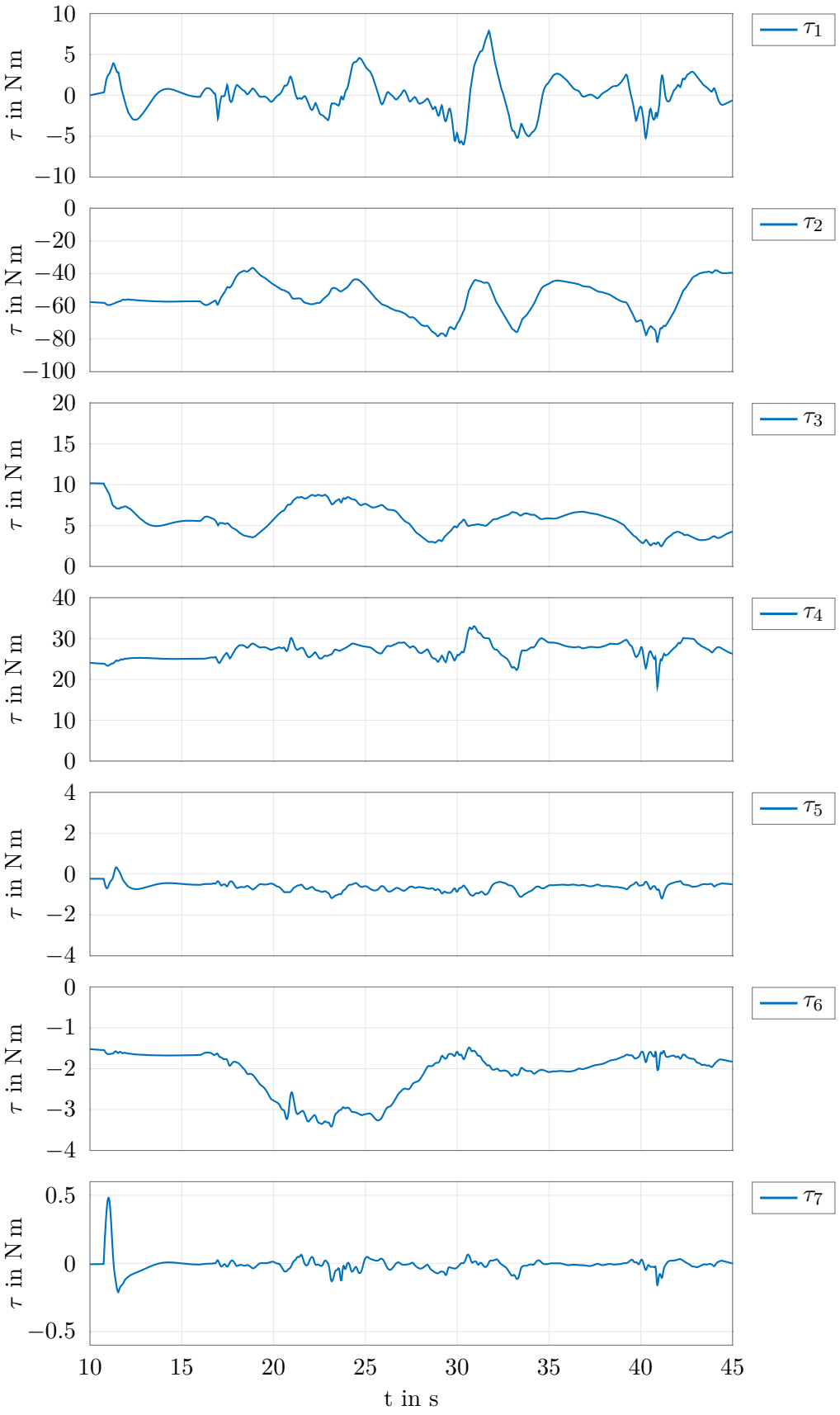

Figure 5.13: Torques per axis in the simulation.

Die approbierte gedruckte Originalversion dieser Diplomarbeit ist an der TU Wien Bibliothek verfügbar.
The approved original version of this thesis is available in print at TU Wien Bibliothek.
TU Bibliothek Your knowledge hub WIEN

5.4 Experimental Results

In this section, the experimental results are presented.

After post-processing the path is provided to the PFC in MATLAB/Simulink. The controller parameters for the experiment are listed in Appendix A.1.5. These PFC parameters were set to achieve small control errors while keeping the torques within their limits despite the external force acting on the end-effector due to the rope tension. The null space parameters are set rather conservative to prevent extensive null space motion.

The desired arc length η^d is set prior to reenactment and defines the target distance that is covered during the process. Figure 5.14 shows η^d, $\dot{\eta}^d$ and $\ddot{\eta}^d$ as outputs of the set-point filter. The second plot shows the speed which is limited to a desired maximum value v_{max} whereas the third plot represents the acceleration.

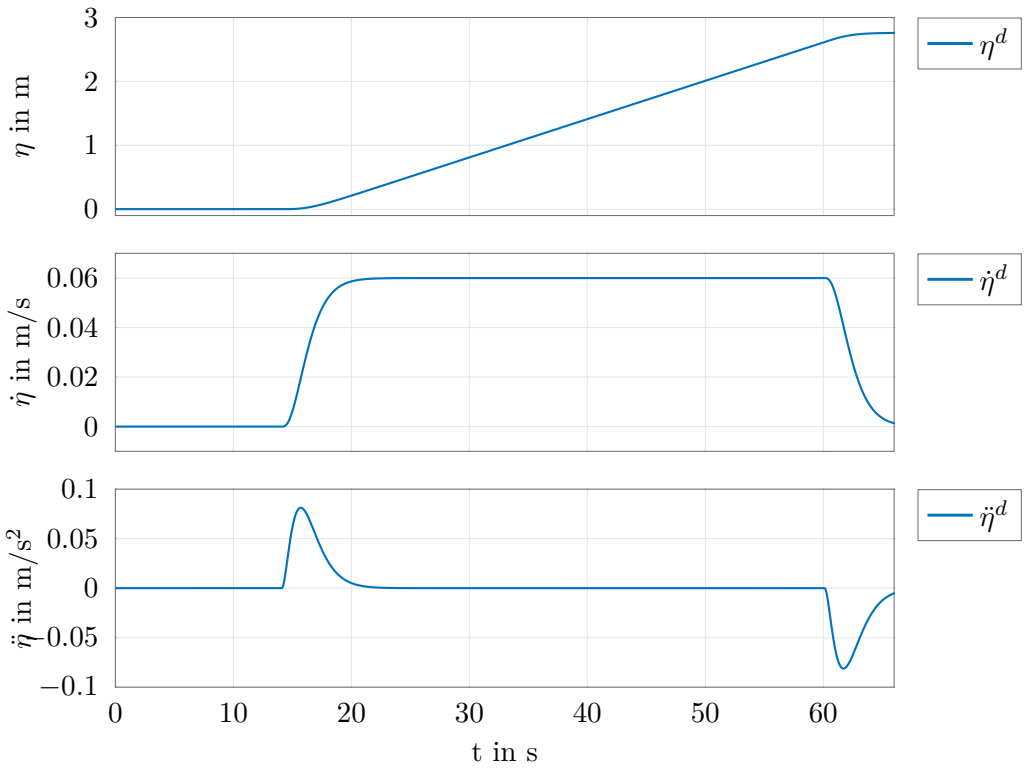

Figure 5.14: Desired trajectory of η.

The error signals in Figure 5.15 show the deviations during the reenactment phase. It can be seen that the combination of feedforward and compliance controller provides good results regarding accurate tracking, in particular when considering that the rope tension acts as an additional external disturbance. This behavior can be observed at the end of the measurement ($t = 56\,\mathrm{s}$) where the tangential error e_η increases due to a larger rope tension being applied. The transversal errors remain small since the pulling force acts in transversal direction. The corresponding motor torque is depicted in Figure 5.16.

Die approbierte gedruckte Originalversion dieser Diplomarbeit ist an der TU Wien Bibliothek verfügbar.
The approved original version of this thesis is available in print at TU Wien Bibliothek.
TU Bibliothek Your knowledge hub WIEN

The initial pose, as controlled by another controller, has a significant error, see Figure 5.15 until $t = 6\,\mathrm{s}$. This constant error results from the TCP not being perfectly aligned with the start position of the path. After switching to the PFC the error declines to zero. The following excitation at $t = 11.8\,\mathrm{s}$ results from the motor which tensions the rope with the initial torque. The motion along the path is started at $t = 14.5\,\mathrm{s}$, compare Figure 5.14.

The second plot in Figure 5.15 shows the orientation error around the x-axis and y-axis. These signals describe two entries of the vector part of the error quaternion, see Section 4.5, hence no unit is written on the ordinate. The difference angle Δ_r of the z-axis is depicted in the third plot, which shows the difference angle in rad between the z-rotation during teach-in and reenactment. As described in Chapter 4, this motion is carried out in the null space. Due to the applied control strategy the z-axis is not restricted to follow the desired z-orientation.

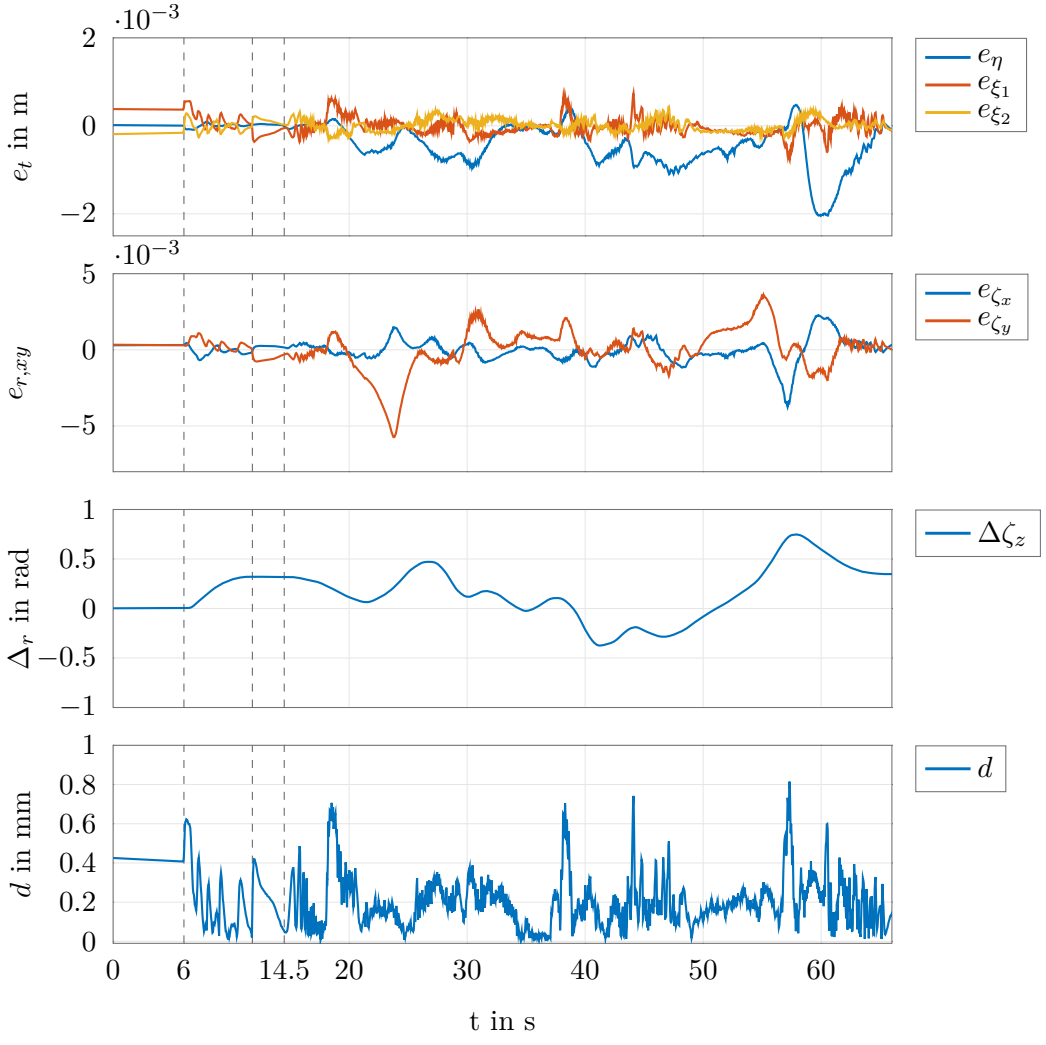

Figure 5.15: Control errors and distance from path during the experiment.

Die approbierte gedruckte Originalversion dieser Diplomarbeit ist an der TU Wien Bibliothek verfügbar.
The approved original version of this thesis is available in print at TU Wien Bibliothek.
TU Bibliothek Your knowledge hub WIEN

Additionally, the Euclidean distance between the end-effector position and the desired position $d = \left\|\mathbf{x} - \mathbf{x}^d\right\|$ is depicted in the last plot of Figure 5.15. As can be seen, the TCP is close to the path during the whole motion despite some small disturbances caused by the rope tension.

Figure 5.16 depicts the torque signal provided to the motor on the flange of the robot. The step at the beginning marks the moment when the motor is switched on. When comparing this signal to the previous control error signals in Figure 5.15 the effects of the applied torque and hence the rope tension are noticeable. This is visible especially for sections with rapid changes in the torque signal.

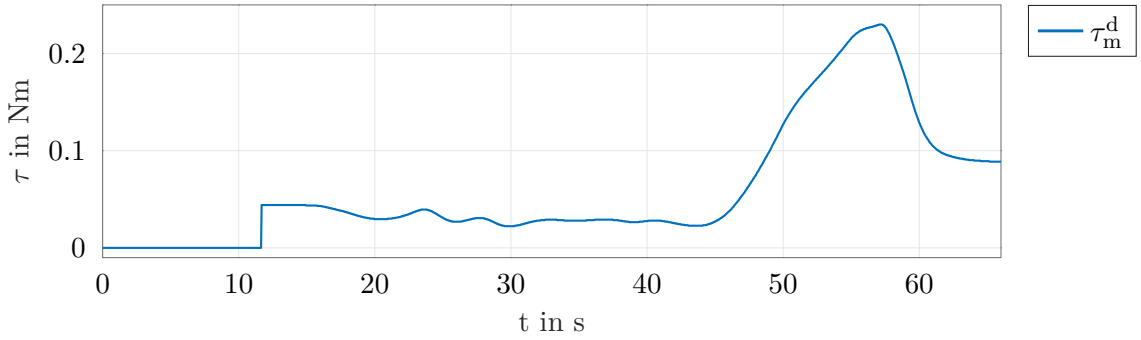

Figure 5.16: Desired spool torque along the path.

The progression of the path parameter θ is depicted in Figure 5.17. The shape results from the calculated optimization steps in Section 4.6.

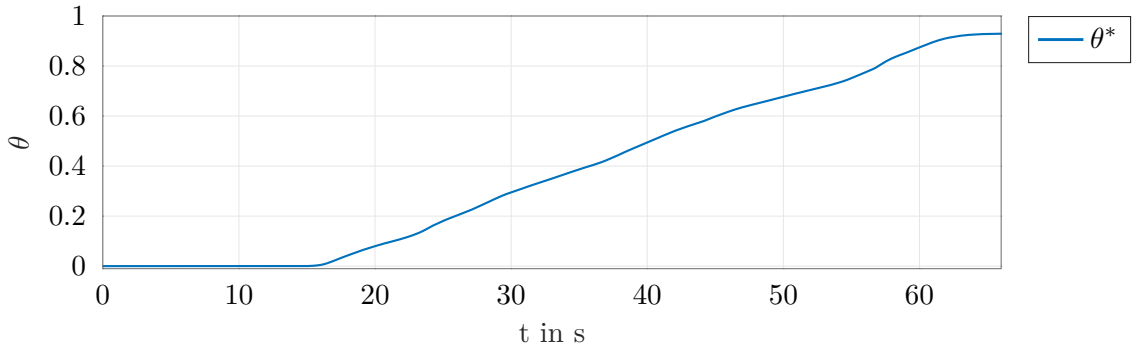

Figure 5.17: Path parameter θ over time.

The joint movements are depicted in Figure 5.18 with the joint limits for each axis drawn as dashed lines. Due to the experimental setup with the rods being placed on a panel next to the robot and the shape of the path, the axis q_4 ("elbow") has to perform a large part of the motion, approaching its joint limit quite regularly. This needs to be considered during the teach-in process.

In the movement of joint q_7, the null space motion can be observed. The initial joint angle results from the starting position that is set before enabling the PFC. Once the PFC is enabled the joint angle approaches zero since the null space controller tries to bring all

Die approbierte gedruckte Originalversion dieser Diplomarbeit ist an der TU Wien Bibliothek verfügbar.
The approved original version of this thesis is available in print at TU Wien Bibliothek.
TU Bibliothek Your knowledge hub WIEN

axes to their neutral position, see Section 4.3. If the spool were mounted vertically on the flange of the robot, axis q_7 would converge to zero once the PFC is enabled and remain there for the whole motion. Since this axis is only able to control the z-rotation of the spool, which is not desired in the primary control task, no motion would be performed. However, due to the tilted spool, axis q_7 has to perform a motion to align the x- and y-rotation of the spool.

The torques for the different axes are plotted in Figure 5.19. They result from the calculated feedback transformation as stated in (4.34) in combination with the control law (4.37). When comparing the joint torques to the maximum torques, listed in Appendix A.1.1, it can be seen that all values are within their limits.

The estimated external torques are depicted in Figure 5.20. The torques of axes q_1, q_3 and q_5 show the effect of the motor stretching the rope at the end of the time interval. In this part, the time evaluation takes the shape of the torque curve in Figure 5.16.

The scenario after the reenactment phase is depicted in Figure 5.10. As can be seen, the rope is wound around the rods as in the demonstration with the desired rope tension applied, see Section 5.1 for a comparison with the teach-in process in Figure 5.2 and the prepared path in Figure 5.6.

Die approbierte gedruckte Originalversion dieser Diplomarbeit ist an der TU Wien Bibliothek verfügbar.
The approved original version of this thesis is available in print at TU Wien Bibliothek.
TU Bibliothek Your knowledge hub WIEN

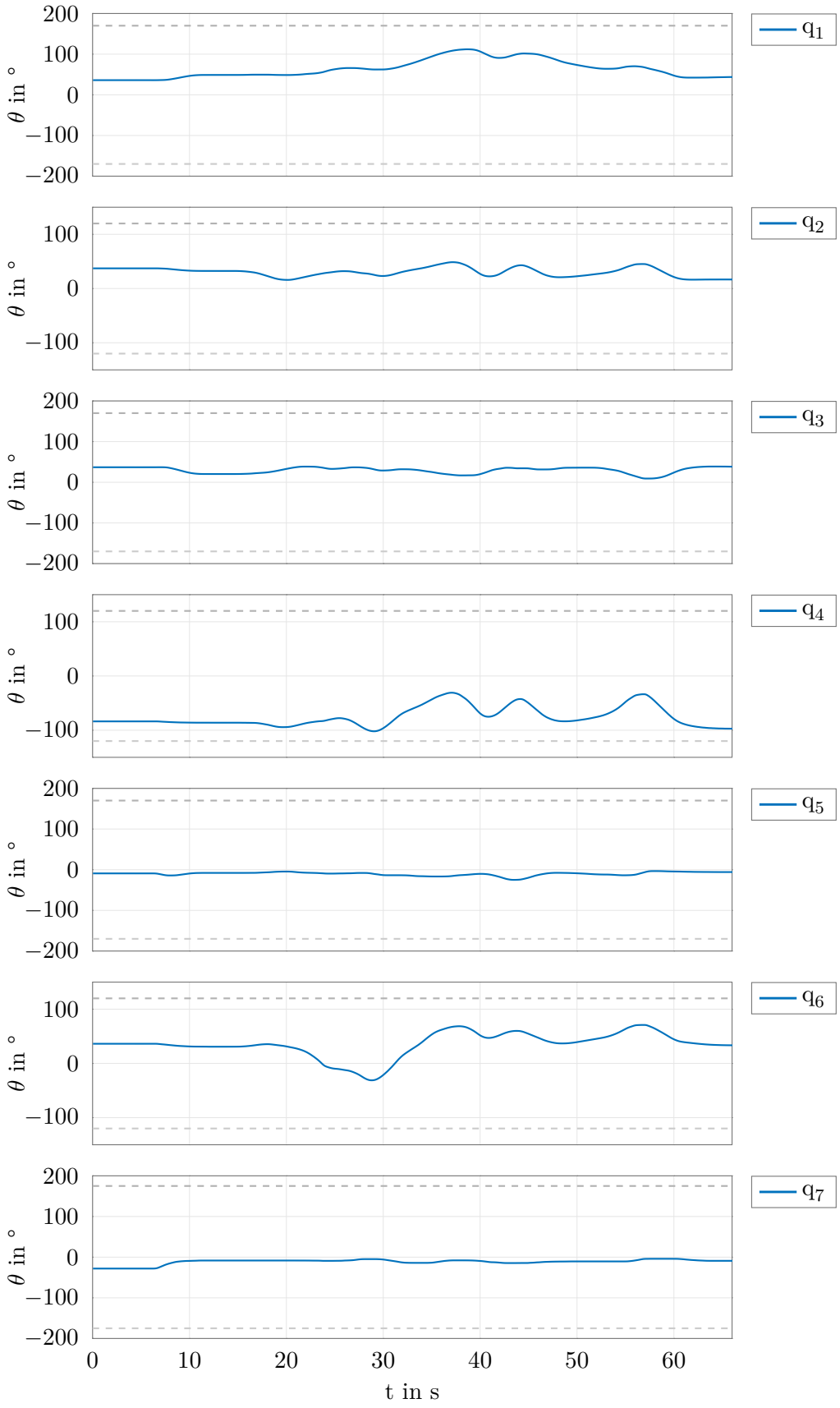

Figure 5.18: Joint angles during reenactment of the task with joint limits (dashed lines).

Die approbierte gedruckte Originalversion dieser Diplomarbeit ist an der TU Wien Bibliothek verfügbar.
The approved original version of this thesis is available in print at TU Wien Bibliothek.
TU Bibliothek Your knowledge hub WIEN

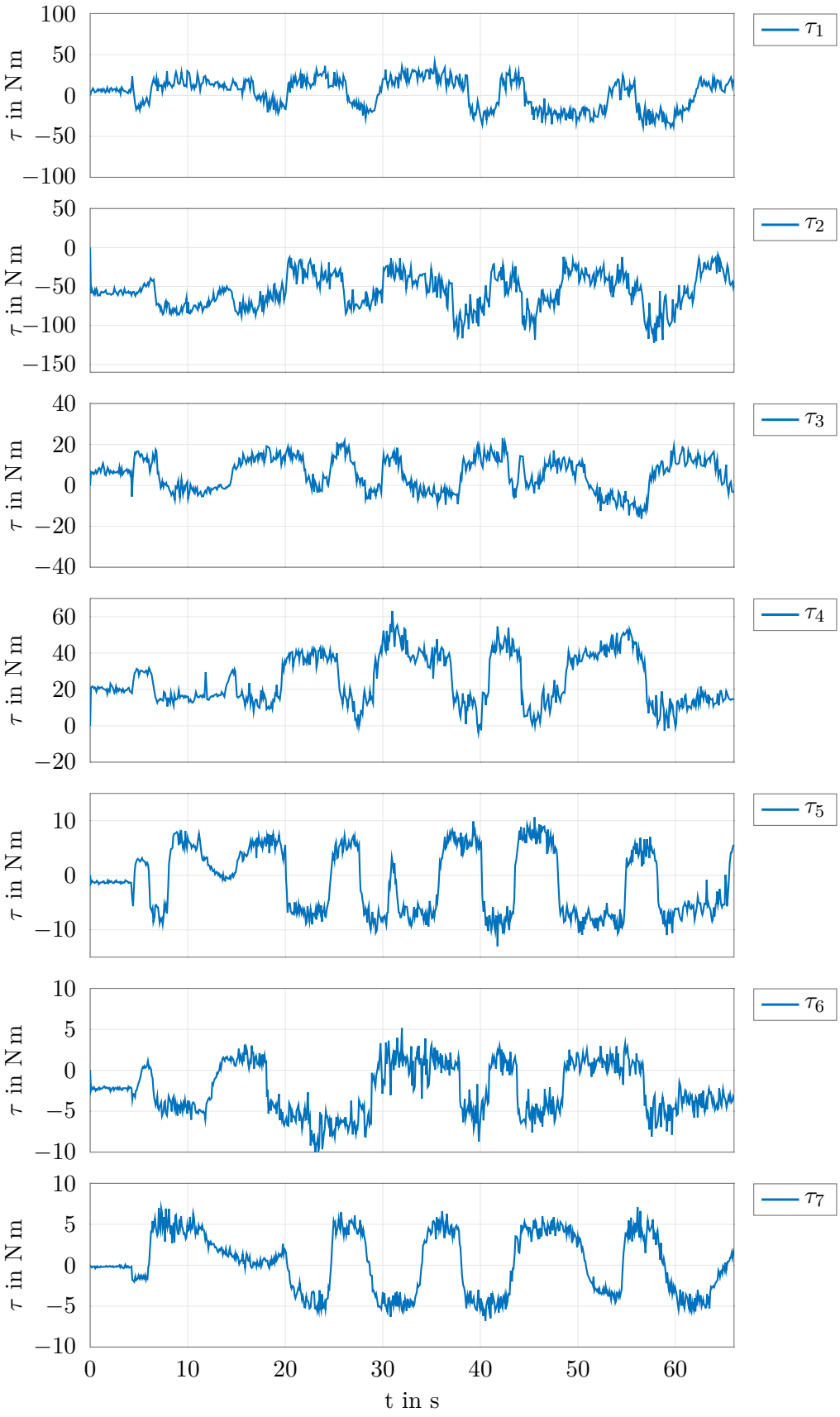

Figure 5.19: Torques resulting from the path following controller during reenactment of the task.

Die approbierte gedruckte Originalversion dieser Diplomarbeit ist an der TU Wien Bibliothek verfügbar.
The approved original version of this thesis is available in print at TU Wien Bibliothek.
TU Bibliothek Your knowledge hub WIEN

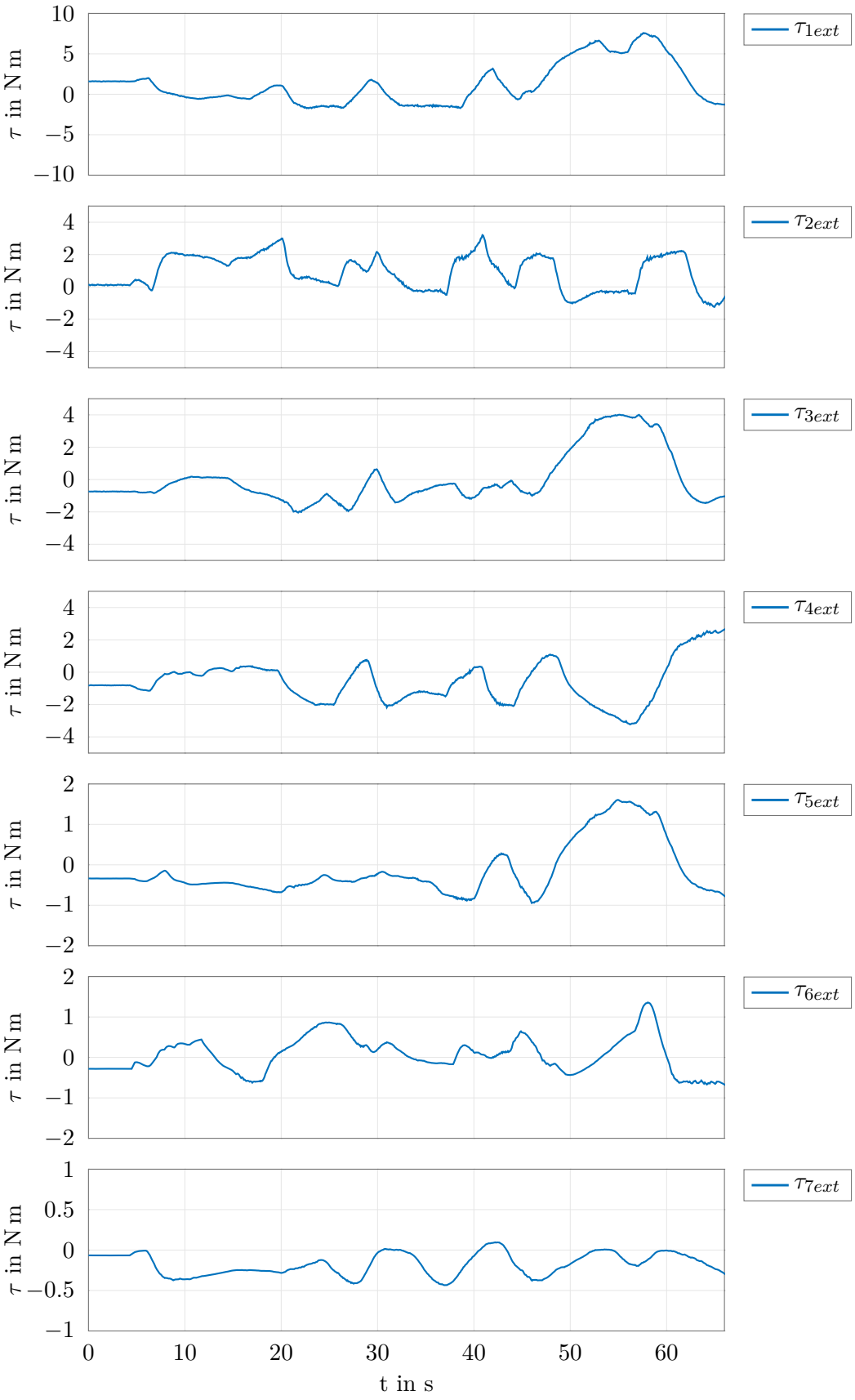

Figure 5.20: Estimated torques due to external forces during reenactment.

Die approbierte gedruckte Originalversion dieser Diplomarbeit ist an der TU Wien Bibliothek verfügbar.
The approved original version of this thesis is available in print at TU Wien Bibliothek.
TU Bibliothek Your knowledge hub WIEN

6 Conclusion and Future Work

In this work, a method for force sensitive teach-in for industrial robots was presented. A teach-in tool was designed that combines the measurement of the tool pose and the tension force along that path. It enables the intuitive demonstration of a rope-winding task. Additionally, a path following control (PFC) concept with a reduced task space was developed which serves as the basis for the reenactment phase.

After derivation of the forward kinematic model in Chapter 2, differential kinematics was used to obtain the manipulator Jacobian matrices. The resulting findings were used in the derivation of the dynamical model of the robot using the Euler-Lagrange equations. Additionally, the singular perturbation theory was applied to account for the elastic joints of the structure.

The designed teach-in tool was introduced in Chapter 3. A rotary torque sensor is integrated into the tool to measure the rope tension and an OPTITRACK system was used to measure the position and orientation of the tool in space. The tool provides an intuitive way to program a robot task by combining position, orientation and force information.

The control strategy is presented in Chapter 4. A parallel transport (PT) frame was used to construct a local coordinate system in every point of the path. The resulting basis vectors were used to transform the output space of the robot to the newly constructed frame. This enables the control of the tool center point of the robot relative to the path. Feedback linearization was employed to obtain an exact linear input-output system forming an integrator chain of length two. This allows to separate the control of the tangential and transversal motion as well as of the orientation. Typically, a 7 degree of freedom (DOF) serial robot has a null space of dimension one allowing the motion of the arm while its end-effector remains fixed. In this work, the null space was extended to two dimensions by moving the rotation around the z-axis of the spool to the null space.

Chapter 5 deals with the implementation and the simulation and experimental results. The post-processing of teach-in trajectories was discussed, explaining how the path was synchronized, smoothed and transformed to get the resulting spline for the PFC. Finally, the utilized hardware setup was presented.

As a result, it was shown that the presented workflow, using the designed teach-in tool, facilitates the teach-in of a rope-winding task considerably. The used PFC strategy was able to follow the demonstrated path while compensating the forces resulting from the applied rope tension. The introduced extension of the null space facilitates the reenactment since the robot configuration does not need to follow the z-rotation of the spool. Additionally, the joints are kept near their neutral position by the null space controller, avoiding unfavorable configurations of the robot.

Die approbierte gedruckte Originalversion dieser Diplomarbeit ist an der TU Wien Bibliothek verfügbar.
The approved original version of this thesis is available in print at TU Wien Bibliothek.
TU Bibliothek Your knowledge hub WIEN

When demonstrating the task, the operator needs to take into account the workspace of the robot. If the teach-in tool is moved close to the edge of the workspace even small changes in the orientation can result in a violation of a joint limit.

In addition, a methodology to either prevent the operator from leaving the workspace during teach-in or to interpret the provided path within the workspace might prove to be a further useful extension.

Die approbierte gedruckte Originalversion dieser Diplomarbeit ist an der TU Wien Bibliothek verfügbar.
The approved original version of this thesis is available in print at TU Wien Bibliothek.
TU Bibliothek Your knowledge hub WIEN

A Appendix

A.1 Parameters

A.1.1 Robot Parameters

The values applying to the robot are obtained from the datasheet, see [24]. The spool angle α was set to a value that brings along satisfactory results in the simulation. The parameter l_t was determined from CAD data of the end-effector construction, placing the TCP at the center of the spool.

Parameter	Value	
d_1	360	mm
d_3	420	mm
d_5	400	mm
α	$-\pi/6$	rad
l_t	80.5	mm

Table A.1: Parameters used for the robot model.

Parameter	q_1	q_2	q_3	q_4	q_5	q_6	q_7	
$\tau_{i_{max}}$	± 320	± 320	± 176	± 176	± 110	± 40	± 40	N m
$\theta_{i_{max}}$	± 170	± 120	± 170	± 120	± 170	± 120	± 175	°

Table A.2: Max joint torques and max joint angles for the KUKA iiwa.

Die approbierte gedruckte Originalversion dieser Diplomarbeit ist an der TU Wien Bibliothek verfügbar.
The approved original version of this thesis is available in print at TU Wien Bibliothek.
TU Bibliothek Your knowledge hub WIEN

A.1.2 Technical Specifications of the Motor

An *EC 90 flat* brushless DC motor from Maxon Motor AG is used. The motor parameters are obtained from [25]. The controller parameters were determined by an auto-tuning process using the software of the manufacturer.

Parameter	Value	
Nominal Voltage	36	V
Nominal Torque	560	mN m
Nominal Current	4.76	A
Torque Constant	109	mN m/A
P Gain	10.061	V/A
I Gain	0.047	V s/A
Feed Forward	0.755	V/A

Table A.3: Motor parameters and controller parameters for the *EC 90 flat* motor.

A.1.3 Technical Specifications of the Sensor

The parameters of the torque sensor are obtained from [16] and listed in Table A.4.

Parameter	Value	
Measurement range	0 ... 2	N m
Supply voltage	11.5 ... 30	V
Current consumption	200	mA
Voltage output	0 ... ± 5	V

Table A.4: Parameters for the rotary torque sensor.

A.1.4 Tool Geometry

The values used for the transformation from the marker body to the spool center point are listed in Table A.5.

Parameter	Value	
d_x	-0.95	mm
d_y	51	mm
d_z	96.46	mm

Table A.5: Distances from the marker body to the center point of the spool.

Die approbierte gedruckte Originalversion dieser Diplomarbeit ist an der TU Wien Bibliothek verfügbar.
The approved original version of this thesis is available in print at TU Wien Bibliothek.
TU Bibliothek Your knowledge hub WIEN

A.1.5 Controller Parameters

The different values for the controller parameters are listed in this section. Table A.6 shows the parameters used in the simulation while Table A.7 lists the parameters used for the experiment.

Parameter	Value
$\mathbf{K}_{0,t}$	diag([500, 800, 800])
$\mathbf{K}_{1,t}$	diag([6, 9, 9])
$\mathbf{K}_{0,r}$	diag([1000, 1000])
$\mathbf{K}_{1,r}$	diag([12, 12])
$\mathbf{K}_{N0}$	diag([4, 4, 4, 4, 4, 4, 4])
$\mathbf{K}_{N1}$	diag([2, 2, 2, 2, 2, 2, 2])
$\mathbf{K}_{\tau}$	diag([4, 4, 4, 5, 3, 2.5, 2.5])
$\mathbf{B}$	diag([10.9, 10.9, 5.9, 5.9, 1.5, 0.45, 0.45])

Table A.6: Controller parameters used in the simulation.

Parameter	Value
$\mathbf{K}_{0,t}$	diag([300, 600, 600])
$\mathbf{K}_{1,t}$	diag([40, 70, 70])
$\mathbf{K}_{0,r}$	diag([800, 800])
$\mathbf{K}_{1,r}$	diag([120, 120])
$\mathbf{K}_{N0}$	diag([2, 2, 2, 2, 2, 2, 2])
$\mathbf{K}_{N1}$	diag([1, 1, 1, 1, 1, 1, 1])
$\mathbf{K}_{\tau}$	diag([4, 4, 4 ,5, 3, 2.5, 2.5])
$\mathbf{B}$	diag([10.9, 10.9, 5.9, 5.9, 1.5, 0.45, 0.45])

Table A.7: Controller parameters used in the experiment.

Die approbierte gedruckte Originalversion dieser Diplomarbeit ist an der TU Wien Bibliothek verfügbar.
The approved original version of this thesis is available in print at TU Wien Bibliothek.
TU Bibliothek Your knowledge hub WIEN

A.2 Teach-In Tool – Technical Drawings

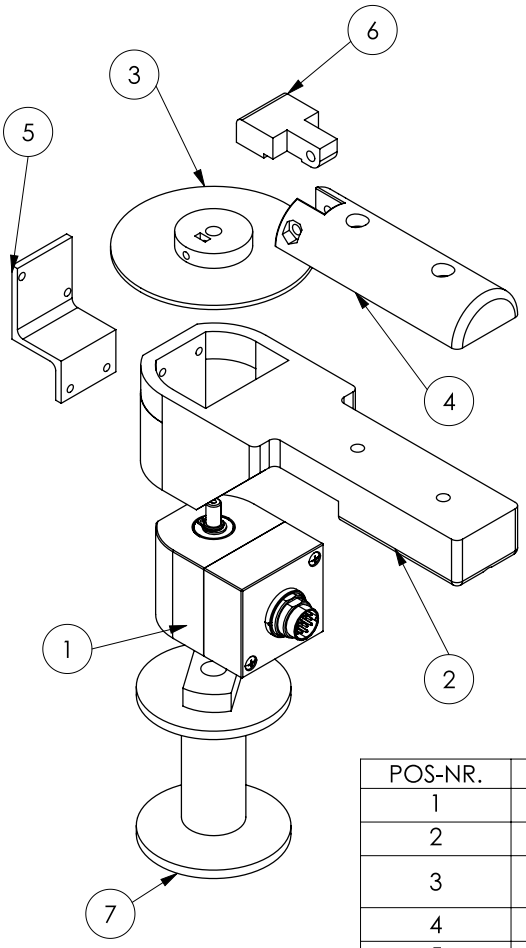

POS-NR.	PART	AMOUNT
1	rotary torque sensor	1
2	tool body	1
3	brake disk	1
4	handle mount	1
5	marker body mount	1
6	brake handle	1
7	spool	1

Figure A.1: Exploded view drawing of the teach-in tool with parts assigned.

Die approbierte gedruckte Originalversion dieser Diplomarbeit ist an der TU Wien Bibliothek verfügbar.
The approved original version of this thesis is available in print at TU Wien Bibliothek.
TU Bibliothek Your knowledge hub WIEN

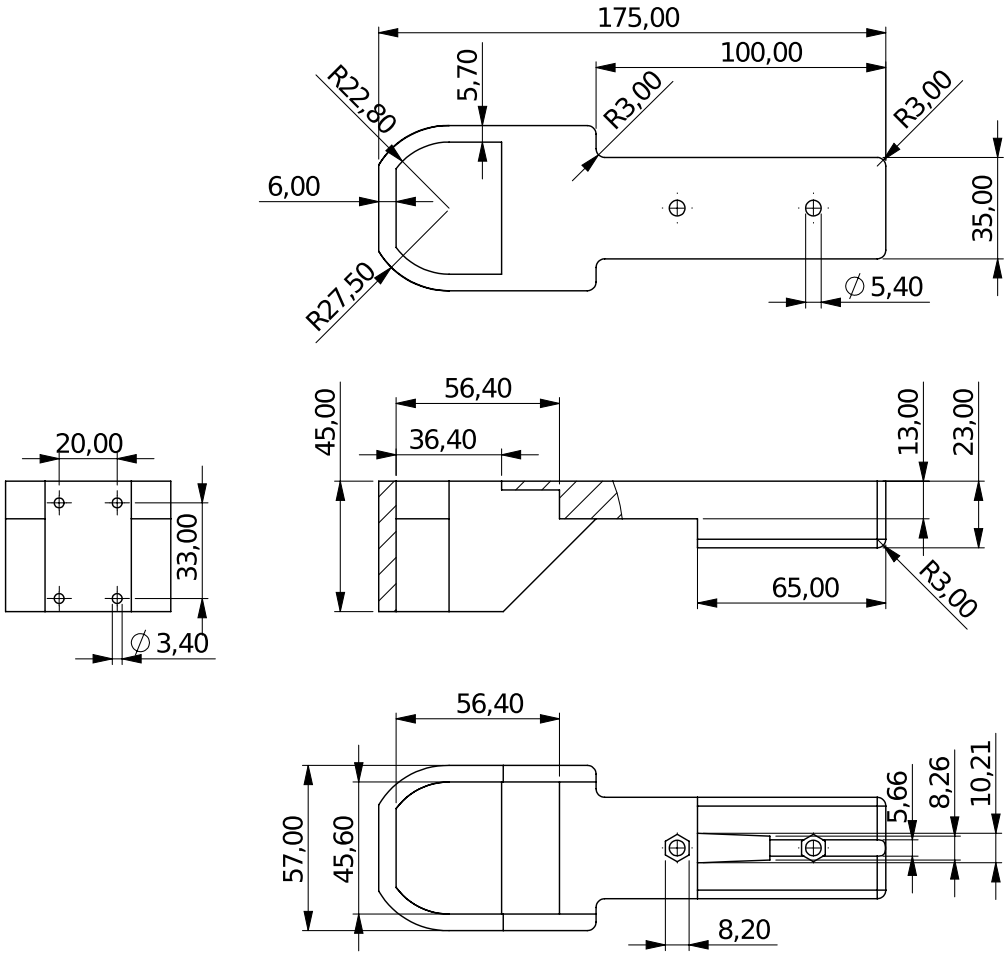

Figure A.2: Body of teach-in tool. All dimensions in mm.

Die approbierte gedruckte Originalversion dieser Diplomarbeit ist an der TU Wien Bibliothek verfügbar.
The approved original version of this thesis is available in print at TU Wien Bibliothek.
TU Bibliothek Your knowledge hub WIEN

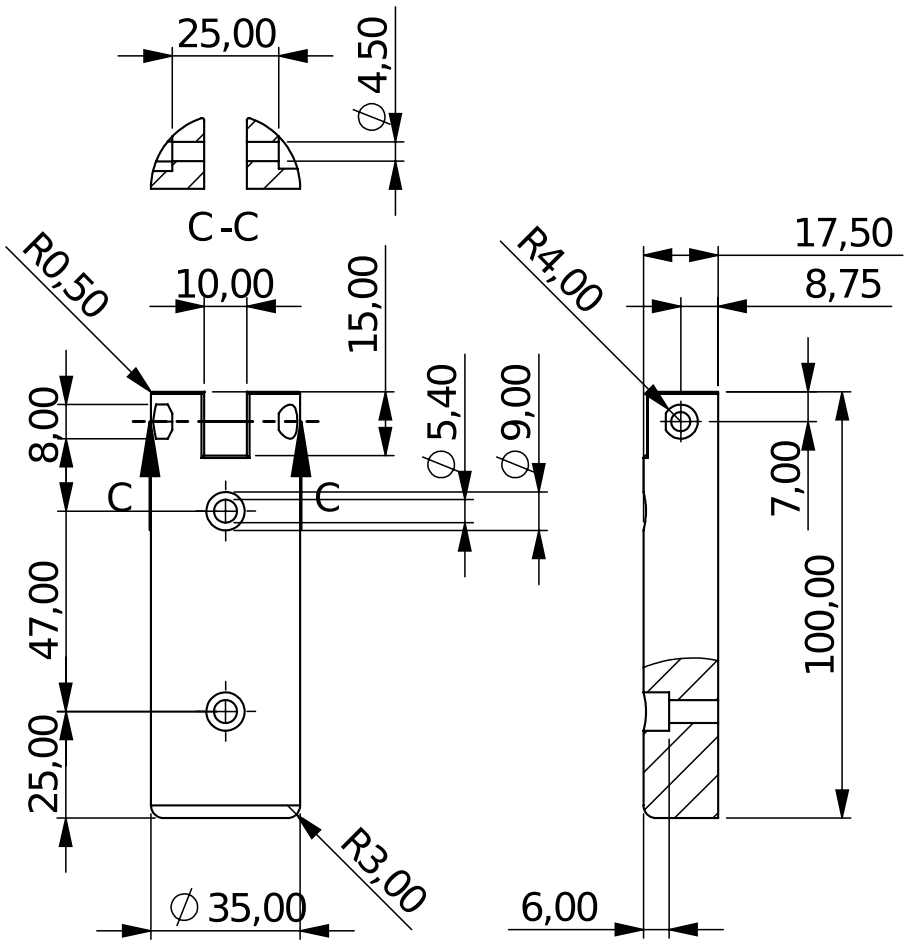

Figure A.3: Handle mount. All dimensions in mm.

Die approbierte gedruckte Originalversion dieser Diplomarbeit ist an der TU Wien Bibliothek verfügbar.
The approved original version of this thesis is available in print at TU Wien Bibliothek.
TU Bibliothek Your knowledge hub WIEN

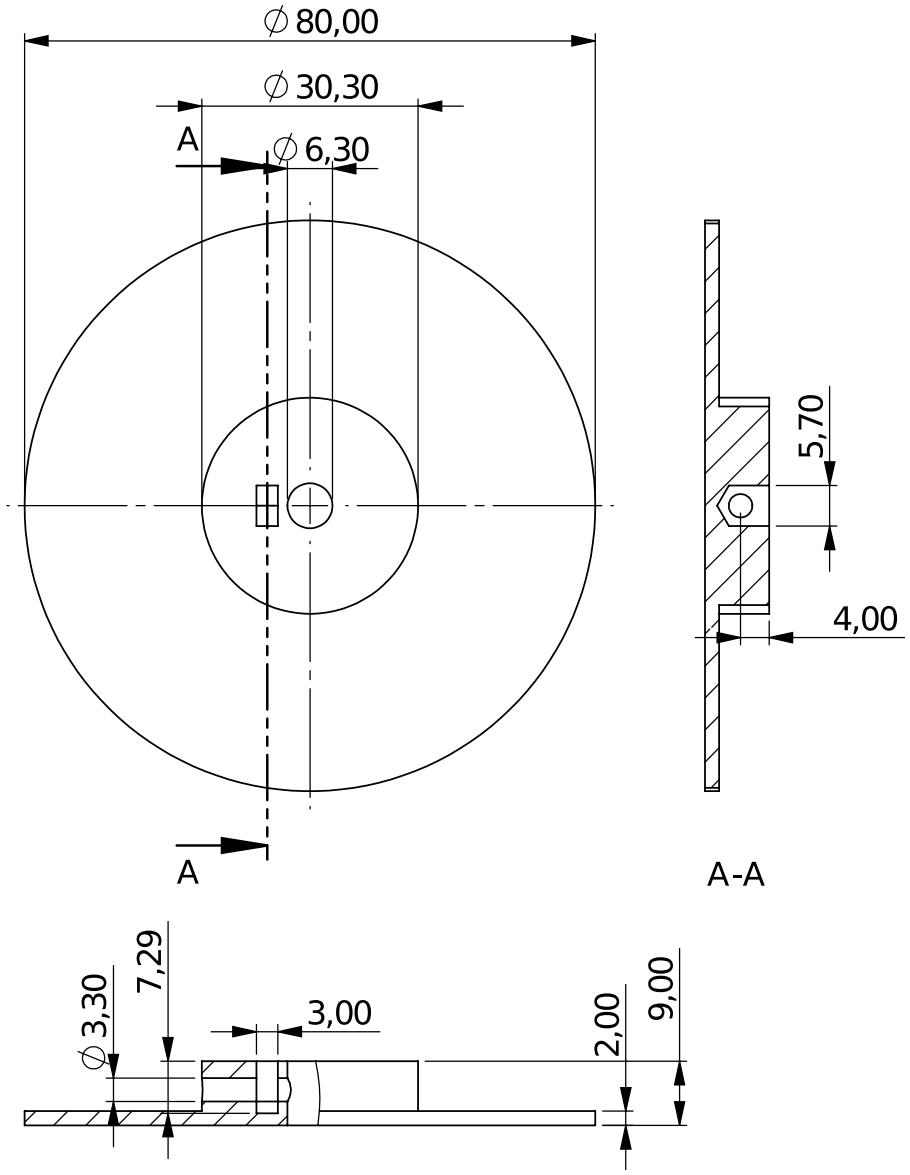

Figure A.4: Brake disk. All dimensions in mm.

Die approbierte gedruckte Originalversion dieser Diplomarbeit ist an der TU Wien Bibliothek verfügbar.
The approved original version of this thesis is available in print at TU Wien Bibliothek.

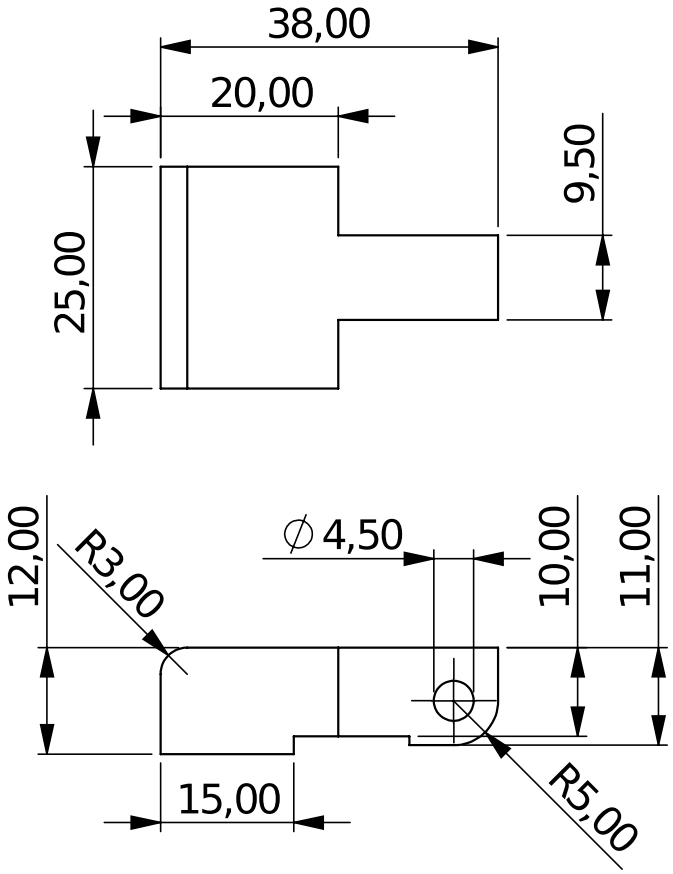

Figure A.5: Brake handle. All dimensions in mm.

Die approbierte gedruckte Originalversion dieser Diplomarbeit ist an der TU Wien Bibliothek verfügbar.
The approved original version of this thesis is available in print at TU Wien Bibliothek.
TU Bibliothek Your knowledge hub WIEN

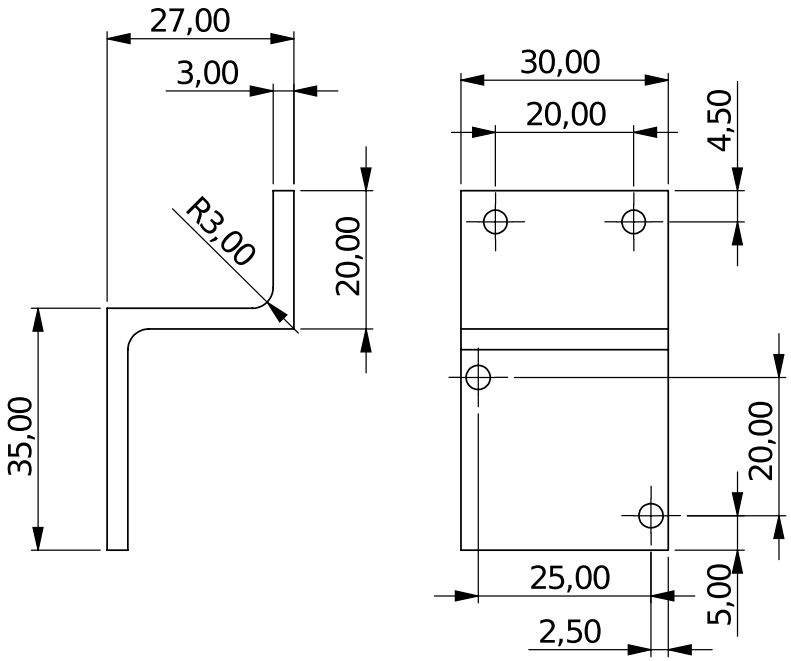

Figure A.6: Marker body mount. All dimensions in mm.

Die approbierte gedruckte Originalversion dieser Diplomarbeit ist an der TU Wien Bibliothek verfügbar.
The approved original version of this thesis is available in print at TU Wien Bibliothek.
TU Bibliothek Your knowledge hub WIEN

Bibliography

[1] A. Billard, S. Calinon, R. Dillmann, and S. Schaal, "Robot Programming by Demonstration," in *Springer Handbook of Robotics*, B. Siciliano and O. Khatib, Eds. Berlin, Heidelberg: Springer, 2008, pp. 1371–1394. [Online]. Available: `https://doi.org/10.1007/978-3-540-30301-5_60` (visited on 02/26/2020).

[2] D. Antonelli, S. Astanin, M. Galetto, and L. Mastrogiacomo, "Training by demonstration for welding robots by optical trajectory tracking," *Procedia Cirp*, vol. 12, pp. 145–150, 2013.

[3] A. Montebelli, F. Steinmetz, and V. Kyrki, "On Handing Down our Tools to Robots: Single-Phase Kinesthetic Teaching for Dynamic In-Contact Tasks," in *2015 IEEE International Conference on Robotics and Automation (ICRA)*, 2015, pp. 5628–5634.

[4] F. Steinmetz, A. Montebelli, and V. Kyrki, "Simultaneous Kinesthetic Teaching of Positional and Force Requirements for Sequential In-Contact Tasks," in *2015 IEEE International Conference on Humanoid Robots (Humanoids)*, 2015, pp. 202–209.

[5] S. Akkaladevi, A. Pichler, M. Plasch, M. Ikeda, and M. Hofmann, "Skill-based programming of complex robotic assembly tasks for industrial application," *e & i Elektrotechnik und Informationstechnik*, vol. 136, pp. 326–333, 2019.

[6] A. Banaszuk and J. Hauser, "Feedback Linearization of Transverse Dynamics for Periodic Orbits," in *1994 IEEE Conference on Decision and Control*, vol. 2, 1994, pp. 1639–1644.

[7] C. Nielsen, C. Fulford, and M. Maggiore, "Path Following Using Transverse Feedback Linearization: Application to a Maglev Positioning System," in *2009 American Control Conference*, 2009, pp. 3045–3050.

[8] A. Hladio, C. Nielsen, and D. Wang, "Path Following for a Class of Mechanical Systems," *IEEE Transactions on Control Systems Technology*, vol. 21, no. 6, pp. 2380–2390, 2013.

[9] R. J. Gill, D. Kulić, and C. Nielsen, "Spline Path Following for Redundant Mechanical Systems," *IEEE Transactions on Robotics*, vol. 31, no. 6, pp. 1378–1392, 2015.

[10] B. Bischof, T. Glück, and A. Kugi, "Combined Path Following and Compliance Control for Fully Actuated Rigid Body Systems in 3-D Space," *IEEE Transactions on Control Systems Technology*, vol. 25, no. 5, pp. 1750–1760, 2017.

[11] C. Hartl-Nesic, B. Bischof, T. Glück, and A. Kugi, "Pfadfolgeregelung mit Konzepten für den Pfadfortschritt: Ein Assemblierungsszenario," *at - Automatisierungstechnik*, vol. 68, no. 1, pp. 44–57, 2019.

[12] A. Haddadi, "Robotic Rope Winding," Master's thesis, Automation and Control Institute (ACIN), TU Wien, 2018.

Die approbierte gedruckte Originalversion dieser Diplomarbeit ist an der TU Wien Bibliothek verfügbar.
The approved original version of this thesis is available in print at TU Wien Bibliothek.
TU Bibliothek Your knowledge hub WIEN

[13] M. W. Spong, S. Hutchinson, and M. Vidyasagar, *Robot Dynamics and Control*, 2nd ed. John Wiley & Sons, 2004. [Online]. Available: `http://home.deib.polimi.it/gini/robot/docs/spong.pdf` (visited on 02/26/2020).

[14] B. Siciliano, L. Sciavicco, L. Villani, and G. Oriolo, *Robotics: Modelling, Planning and Control*. London: Springer, 2009.

[15] C. Ott, *Cartesian Impedance Control of Redundant and Flexible-Joint Robots*. Springer, 2008, vol. 49. [Online]. Available: `http://dx.doi.org/10.1007/978-3-540-69255-3_3` (visited on 02/26/2020).

[16] *Drehmomentaufnehmer DRBK + DRBK-A*, ETH-Messtechnik. [Online]. Available: `https://www.eth-messtechnik.de/_datenblaetter/Datenblatt_Drehmomentsensor_DRBK-DRBK-A.pdf` (visited on 02/26/2020).

[17] Optitrack. (2020). Prime 17w - technical specifications, [Online]. Available: `https://optitrack.com/products/prime-17w/specs.html` (visited on 02/26/2020).

[18] V. A. Toponogov, *Differential Geometry of Curves and Surfaces - A Concise Guide*. Boston: Birkhäuser, 2006.

[19] R. L. Bishop, "There is More than One Way to Frame a Curve," *The American Mathematical Monthly*, vol. 82, no. 3, pp. 246–251, 1975. [Online]. Available: `http://www.jstor.org/stable/2319846` (visited on 02/26/2020).

[20] A. Dietrich, C. Ott, and A. Albu-Schäffer, "An Overview of Null Space Projections for Redundant, Torque-Controlled Robots," *The International Journal of Robotics Research*, vol. 34, no. 11, pp. 1385–1400, 2015.

[21] J. S. Yuan, "Closed-Loop Manipulator Control using Quaternion Feedback," *IEEE Journal on Robotics and Automation*, vol. 4, no. 4, pp. 434–440, 1988.

[22] M.-J. Kim, M.-S. Kim, and S. Shin, "A C2-continous B-spline Quaternion Curve Interpolating a Given Sequence of Solid Orientations," in *Proceedings Computer Animation*, 1995, pp. 72–81.

[23] ——, "General Construction Scheme for Unit Quaternion Curves with Simple High Order Derivatives," in *SIGGRAPH*, 1995, pp. 369–376.

[24] *KUKA LBR iiwa 7 R800, LBR iiwa 14 R820 Specification*, 8th ed., KUKA GmbH, 2019.

[25] *Ec 90 flat, brushless, 90 Watt*, Maxon Motor AG, 2017. [Online]. Available: `https://www.maxongroup.com/medias/sys_master/8825435389982.pdf` (visited on 02/26/2020).

Die approbierte gedruckte Originalversion dieser Diplomarbeit ist an der TU Wien Bibliothek verfügbar.
The approved original version of this thesis is available in print at TU Wien Bibliothek.
TU Bibliothek Your knowledge hub WIEN

Eidesstattliche Erklärung

Hiermit erkläre ich, dass die vorliegende Arbeit gemäß dem Code of Conduct – Regeln zur Sicherung guter wissenschaftlicher Praxis (in der aktuellen Fassung des jeweiligen Mitteilungsblattes der TU Wien), insbesondere ohne unzulässige Hilfe Dritter und ohne Benutzung anderer als der angegebenen Hilfsmittel, angefertigt wurde. Die aus anderen Quellen direkt oder indirekt übernommenen Daten und Konzepte sind unter Angabe der Quelle gekennzeichnet. Die Arbeit wurde bisher weder im In– noch im Ausland in gleicher oder in ähnlicher Form in anderen Prüfungsverfahren vorgelegt.

Vienna, February 2020

Hanspeter Augschöll

Die approbierte gedruckte Originalversion dieser Diplomarbeit ist an der TU Wien Bibliothek verfügbar.
The approved original version of this thesis is available in print at TU Wien Bibliothek.
TU Bibliothek Your knowledge hub WIEN